

ANTENNA DESIGN FOR UHF RFID TRANSPONDER

by

Radu Radu

Submitted

in partial fulfillment of the requirements

for the degree of

MASTER OF ENGINEERING

Major Subject: Electrical and Computer Engineering/Graduate Studies

at

DALHOUSIE UNIVERSITY

Halifax, Nova Scotia

December, 2008

© Copyright by Radu Radu, 2008



Library and
Archives Canada

Bibliothèque et
Archives Canada

Published Heritage
Branch

Direction du
Patrimoine de l'édition

395 Wellington Street
Ottawa ON K1A 0N4
Canada

395, rue Wellington
Ottawa ON K1A 0N4
Canada

Your file Votre référence
ISBN: 978-0-494-50038-5
Our file Notre référence
ISBN: 978-0-494-50038-5

NOTICE:

The author has granted a non-exclusive license allowing Library and Archives Canada to reproduce, publish, archive, preserve, conserve, communicate to the public by telecommunication or on the Internet, loan, distribute and sell theses worldwide, for commercial or non-commercial purposes, in microform, paper, electronic and/or any other formats.

The author retains copyright ownership and moral rights in this thesis. Neither the thesis nor substantial extracts from it may be printed or otherwise reproduced without the author's permission.

AVIS:

L'auteur a accordé une licence non exclusive permettant à la Bibliothèque et Archives Canada de reproduire, publier, archiver, sauvegarder, conserver, transmettre au public par télécommunication ou par l'Internet, prêter, distribuer et vendre des thèses partout dans le monde, à des fins commerciales ou autres, sur support microforme, papier, électronique et/ou autres formats.

L'auteur conserve la propriété du droit d'auteur et des droits moraux qui protègent cette thèse. Ni la thèse ni des extraits substantiels de celle-ci ne doivent être imprimés ou autrement reproduits sans son autorisation.

In compliance with the Canadian Privacy Act some supporting forms may have been removed from this thesis.

Conformément à la loi canadienne sur la protection de la vie privée, quelques formulaires secondaires ont été enlevés de cette thèse.

While these forms may be included in the document page count, their removal does not represent any loss of content from the thesis.

Bien que ces formulaires aient inclus dans la pagination, il n'y aura aucun contenu manquant.

■*■
Canada

DALHOUSIE UNIVERSITY

To comply with the Canadian Privacy Act the National Library of Canada has requested that the following pages be removed from this copy of the thesis:

Preliminary Pages

Examiners Signature Page

Dalhousie Library Copyright Agreement

Appendices

Copyright Releases (if applicable)

TABLE OF CONTENTS

	Page
LIST OF TABLES	vii
LIST OF FIGURES	viii
LIST OF SYMBOLS AND ABBREVIATIONS	x
ACKNOWLEDGEMENTS	xii
ABSTRACT	xiii
1 INTRODUCTION	1
1.1 Passive UHF RFID System Overview	1
1.1.1 Frequency Range	1
1.1.2 Backscattering	2
1.1.3 Power Budget.....	3
1.1.4 Real Environment Operations	5
1.2 Communication Protocol for UHF RFID.....	5
1.2.1 Frequencies and Channel Occupancy.....	6
1.2.2 Reader Modulation and Data Encoding.....	7
1.2.3 Tag Modulation and Data Encoding	8
1.2.4 Data Rate and Bandwidth.....	9
1.2.5 Data Integrity	10
1.3 Transponder Parameters Affecting System Performance	10
1.3.1 Antenna Size and Shape	11
1.3.2 Fabrication Materials and Process	12
1.3.3 Proximity to Objects	13
1.3.4 Tag's Orientation vs. Reader's Antenna	13
1.3.5 Deformation	14
1.3.6 Density and Relative Motion Speed	15
2 REVIEW OF ANTENNA THEORY	16
2.1 Fundamental Parameters of Antennas	16
2.1.1 Radiation Pattern.....	16
2.1.2 Antenna Efficiency	20
2.1.3 Gain	21
2.1.4 Polarization	21
2.1.5 Bandwidth	22
2.1.6 Input Impedance.....	22
2.1.7 Antenna Equivalent Areas.....	23
2.1.8 FRIIS Transmission Equation	24

2.1.9	Antenna Radar Cross Section.....	26
2.2	Broadband Dipoles.....	27
2.3	Peak Power Gain Measurement and Sources of Error	28
3	UHF RFID TRANSPONDER ANTENNA DESIGN	31
3.1	Analysis of Design Inputs	31
3.2	ASIC Impedance	33
3.2.1	Texas Instruments ASIC.....	33
3.2.2	ASIC Impedance Measurement.....	36
3.2.2.1	Setup and Calibration	36
3.2.2.2	Measurement Results.....	38
3.2.2.3	Sources of Error	40
3.2.3	Determination of the Impedance Matching Point.....	42
3.3	Antenna Modeling	43
3.4	Parametric Study	45
3.4.1	Length	45
3.4.2	Width.....	47
3.4.3	Radius of the Loop	48
3.4.4	Width of the Loop Track	49
3.4.5	Thickness and Permittivity of Substrate	50
3.4.6	Final Parameters Chosen for Prototypes.....	52
3.5	Measurement of Antenna Prototypes	55
3.5.1	Measurement of Antenna Impedance.....	56
3.5.1.1	Measurement Results.....	56
3.5.1.2	Sources of Error	59
3.5.2	Measurement of Maximum Gain.....	60
3.5.2.1	Instrument Calibration and Measurement of Offset.....	60
3.5.2.2	Calculation of the Reference Transmission Level	62
3.5.2.3	Measurement Results.....	64
3.5.2.3	Sources of Error	66
3.5.3	Radiation pattern measurement.....	66
3.6	Prototype Transponders Range	69
3.6.1	Range Estimation	69
3.6.2	Range Measurement.....	73
3.6.2.1	Setup and Calibration	75
3.6.2.2	Transponder's Range Measurement Results	81
3.6.2.3	Range of Prototype Transponders in Real Environment	83
3.6.2.4	Analysis of Range Measurement Results	85
4	CONCLUSIONS.....	88
	BIBLIOGRAPHY	91

APPENDIX 1	Conversion of impedance from Parallel to Series configuration.....	93
APPENDIX 2	Calculation of ASIC impedance using Parallel configuration	94
APPENDIX 3	Calculation of datasheet reflection coefficient	95
APPENDIX 4	Measurement of ASIC impedance at five power levels	96
APPENDIX 5	Measured ASIC impedance	97
APPENDIX 6	Measurement of the prototype antennas impedance	98
APPENDIX 7	Measurement of transmission level from horn to probe	99
APPENDIX 8	Transmission coefficient for antennas relative to 50 ohm	100
APPENDIX 9	Transmission level from prototype antennas to probe.....	101

LIST OF TABLES

Table 1	Examples of frequency bands used for UHF RFID systems	1
Table 2	Estimation of power budget for transponder's ASIC	3
Table 3	Estimation of power budget for reader's receiver	4
Table 4	Impedances of TI chip at different frequencies and power levels	34
Table 5	Series impedance for TI chip	34
Table 6	Series impedance for TI ASIC for -13 dBm input power level	35
Table 7	Four prototyping options	53
Table 8	Parameter values for four prototype antennas	53
Table 9	Power transmission coefficient for "Short-M" antenna prototype	59
Table 10	Jumper cable insertion loss	61
Table 11	Chamber cables insertion loss	61
Table 12	Summary of standard antenna transmission measurement	63
Table 13	Reference Transmission Level	64
Table 14	Maximum gain calculation for "Short-M" antenna prototype	65
Table 15	Maximum gain calculation for reader's antenna	69
Table 16	Power transmission coefficient for the "Short-M" transponder	71
Table 17	Range estimation for the "Short-M" transponder	71
Table 18	Reader's output power measurement for linearity verification	79
Table 19	Direct and reflected power on antenna port at different frequencies	80
Table 20	Read range for "Short-D" tag	81
Table 21	Read range for "Short-M" tag	81
Table 22	Read range for "Long-D" tag	81
Table 23	Read range for "Long-M" tag	81
Table 24	Read range for Texas Instruments tag	82
Table 25	Range of prototype transponders in real environment	84

LIST OF FIGURES

Figure 1	UHF RFID system block diagram	2
Figure 2	Pulse Interval Encoding symbols	7
Figure 3	FM0 (Bi-Phase Space) symbols	8
Figure 4	Miller symbols	8
Figure 5	Subcarrier spectral allocation for 902 to 928 MHz band	9
Figure 6	Radiation pattern of a dipole	16
Figure 7	Radiation patterns for a thin small dipole with different lengths	19
Figure 8	Directivity pattern of a $\lambda/2$ dipole in the elevation plane	20
Figure 9	Transmitting and receiving antennas for Friis transmission equation.....	24
Figure 10	Biconical and tapered dipole antenna geometries.....	27
Figure 11	Bow-tie antenna	27
Figure 12	Setup for peak power gain measurement	29
Figure 13	Internal configuration for ASIC's impedance	33
Figure 14	ASIC datasheet impedance variation on the Smith Chart	35
Figure 15	VNA's 1-Port calibration for impedance measurement	36
Figure 16	ASIC impedance measurement	37
Figure 17	Series resistance measured at five power levels for one ASIC.....	38
Figure 18	Series reactance measured at five power levels for one ASIC	39
Figure 19	Average of four ASICs impedance at -13 dBm input power level	40
Figure 20	VNA's calibration error sources	41
Figure 21	Antenna modeling with Ansoft HFSS software package.....	43
Figure 22	Finite air space used for simulation for antenna modeling.....	44
Figure 23	Antenna impedance variation with "Arm" parameter	46
Figure 24	Antenna impedance variation with "L-triangle" parameter.....	46
Figure 25	Antenna impedance variation with "W_triangle" parameter	47
Figure 26	Antenna impedance variation with "R_ring" parameter	49
Figure 27	Antenna impedance variation with "W_track" parameter	50
Figure 28	Antenna impedance variation with FR4 substrate thickness	51
Figure 29	Antenna impedance variation with FR4 substrate relative permittivity.....	51
Figure 30	Parameters that change impedance in nearly orthogonal directions.....	52
Figure 31	Two "Short" antennas impedance variation.....	54
Figure 32	Two "Long" antennas impedance variation.....	54
Figure 33	"Short" transponder antenna - copper layout.....	55
Figure 34	"Long" transponder antenna - copper layout.....	55
Figure 35	Antenna impedance measurement setup.....	56
Figure 36	Impedance of "Long-D" antenna prototype	57
Figure 37	Impedance of "Long-M" antenna prototype	57
Figure 38	Impedance of "Short-D" antenna prototype.....	58
Figure 39	Impedance of "Short-M" antenna prototype	58
Figure 40	Offset measurement setup	61

Figure 41	Transmission calibration setup using a standard antenna	62
Figure 42	Prototype antennas prepared for maximum gain measurement	64
Figure 43	Measured Near-field radiation pattern for “Long-M” antenna prototype ..	67
Figure 44	Measured Near-field radiation pattern for “Short-M” antenna prototype ..	67
Figure 45	Range estimations for all four prototype transponders	72
Figure 46	Prototype transponders.....	73
Figure 47	ASIC attachment to antenna.....	73
Figure 48	Reader mounted to antenna	74
Figure 49	Reader’s interface software control window	75
Figure 50	Setup for transponder range measurement.....	76
Figure 51	Transponder during range measurement	77
Figure 52	Direct and reflected power measurement of the reader assembly	78
Figure 53	Read range measurement for all four prototype transponders	82
Figure 54	RFID system operations in real environment	83
Figure 55	Reader operating with all tags in real environment	84
Figure 56	Recommended range measurement setup	86

LIST OF SYMBOLS AND ABBREVIATIONS

3D	Three Dimensional
ASIC	Application Specific Integrated Circuit
ASK	Amplitude Shift Keying
CMOS	Complementary Metal Oxide Semiconductor
CRC	Cyclic Redundancy Check
CW	Continuous Wave
dB	Decibel
dBc	Decibel relative to Carrier
dB _i	Decibel relative to Isotropic antenna gain
dB _{sm}	Decibel per Square Meter
dB _m	Decibel relative to Mili-watt
DBP	Differential Bi-Phase
DSB-ASK	Double Sided Band ASK
EPC	Electronic Product Code
EIRP	Equivalent Isotropically Radiated Power
ERP	Effective Radiated Power
ESD	Electro Static Discharge
FCC	Federal Communication Commission
FEM	Finite Element Method
FM0	Bi-phase space encoding
FHSS	Frequency Hopping Spread Spectrum
FR4	Flame Retardant 4
GHz	Gigahertz
HDPE	High Density Poly Ethylene
HFSS	High Frequency Simulation Software
HPBW	Half Power Bandwidth
Hz	Hertz
IC	Integrated Circuit
ID	Identification Device
ISM	Industrial Scientific and Medical (radio band)
Kbps	Kilo Bit Per Second
kHz	Kilohertz
MHz	Megahertz
RC	Resistor-Capacitor
PCB	Printed Circuit Board
RCS	Radar Cross Section
PET	Polyethylene Therephthalate
pF	Pico Farad
RF	Radio Frequency
RFID	Radio Frequency Identification Devices

PIE	Pulse-Interval Encoding
PP	Polypropylene
PR-ASK	Phase Reversal ASK
PSK	Phase Shift Keying
SMA	SubMiniature version A connector
SNR	Signal to Noise Ratio
SSB-ASK	Single Sided Band ASK
TI	Texas Instruments
UHF	Ultra High Frequency
VNA	Vector Network Analyzer
VSWR	Voltage Standing Wave Ratio
λ	Wavelength

ACKNOWLEDGEMENTS

I would like to acknowledge the excellent support received from Texas Instruments, in form of ASIC samples and reference documentation. I must express my sincere gratitude to Ken Chaddock, my work supervisor, and to the management of Fleet Maintenance Facility Cape Scott in Halifax Dockyard (DND Canada) for accommodating a flexible work schedule in order to complete the program requirements and this project.

I am forever grateful to Dr. Zhizhang Chen, my academic supervisor, for guidance on completion of this work. I would like to extend the appreciation to all my research associates in the microwave and wireless lab at Dalhousie University for helpful comments and advice. Also, I would like to acknowledge all other people that contributed with input, directly or indirectly, since the beginning of this work.

I must personally thank Charles Mao, my colleague and my friend, for being supportive since the first time we've met, at the beginning of my graduate studies program. Last, but not least, I would like to thank to my loving wife Ardith Carter for accommodations and to my parents Tanta and Oprea for a lifelong dedication to my education and professional career.

ABSTRACT

This project presents a design method for Ultra High Frequency (UHF) Radio Frequency Identification Device (RFID) transponder antenna, which can be used in various tracking applications including assets and personnel. The frequency band of interest is 860 to 960 megahertz (MHz).

The factors that influence the overall performance of an RFID system are studied. They include size and shape of antenna, materials selected for fabrication and proximity of objects from the transponder. They are important design parameters and need to be addressed in the design process.

Ansoft High Frequency Simulation Software (HFSS), a Finite Element Method (FEM) simulation software, is used to compute three-dimensional (3D) electromagnetic fields generated by the antenna model. The results are visualized on a Smith Chart for antenna impedance and on a 3D plot for antenna radiation pattern. The antenna parameters are then optimized, seeking good matching between the antenna and Application Specific Integrated Circuit (ASIC) impedance.

Prototype antennas are developed and tested. Parameters such as antenna input impedance and gain are measured. The results of these measurements are used to compute a reflection coefficient and an estimated range of operation for transponders as variation of frequency. The prototype transponders are built and the operation range tested inside the anechoic chamber. The results verify the design method proposed in this project.

A significant portion of this project is dedicated to the analysis of error sources affecting the measurements. The overall approach is to progress in small steps and ensure verification after each stage of the design. In such a way, understanding and accounting for unpredictable effects can be carried out.

1 INTRODUCTION

1.1 *Passive UHF RFID System Overview*

The Radio Frequency Identification Devices (RFID) systems were introduced as a solution for identification of large volume of objects in a shorter period of time and replacement of classic barcode labels. The perspective of reading multiple identification devices (ID) in a matter of seconds at distances between 3 and 10 ft. stimulated worldwide development.

Starting in 2004, EPC Global Inc. coordinated the efforts to develop and establish an international standard that will bring regulating bodies from different countries to work together. In 2005 the document **Electronic Product Code (EPC)[™] Radio-Frequency Identity Protocols, Class-1 Generation-2 UHF RFID, Protocol for Communications at 860 MHz – 960 MHz** was released. The expectation was that the number of potential users will increase many times and would create a significant demand in this market, driving the costs down.

1.1.1 Frequency Range

The frequency bands available in different regions of the world are different except for the fact that the RFID transponders are designed to operate between 860 to 960 MHz.

Table 1 Examples of frequency bands used for UHF RFID systems

	Europe	North America	Japan
Band	866 – 868 MHz	902 – 928 MHz	952 – 954 MHz
Power	2W ERP	4W EIRP	4W EIRP
Spurious limits	-63 dBc	-50 dBc	-61 dBc

As can be seen from Table 1, the 2 MHz bandwidth available in Europe and Japan is significantly smaller than 26 MHz bandwidth available in North America. As well, the spurious limits in North America are more relaxed than that in Europe and Japan. The direct consequence of these limitations is a lower data rate between reader and transponder in the other regions outside North America.

1.1.2 Backscattering

A basic RFID system consists of a reader connected to an antenna and a transponder. The transponder (called also tag) is fabricated by attaching an Application Specific Integrated Circuit (ASIC) to a antenna. The source of energy for a passive transponder is the electromagnetic field generated at the reader's antenna. For backscattering RFID systems the passive transponder is always operating in the far-field. The operation principle is similar to that of radar [1].

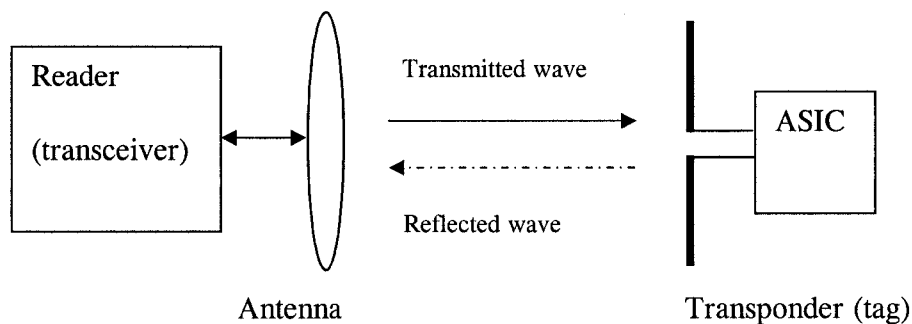


Figure 1 UHF RFID system block diagram

As illustrated in the Figure 1, the reader initiates the communications by sending interrogation messages. The transponder replies to the reader's interrogation by changing the impedance of its antenna, and modulating the amplitude and/or the phase of the reflected wave. Back at the reader, the reflected wave is then received, demodulated and decoded.

Reliable operations of UHF RFID systems over a certain range depend on two principal conditions: sufficient power for the electronics in the transponder and sufficient receiver sensitivity of the reader.

1.1.3 Power Budget

It is important to know which of the operation conditions stated in section 1.1.2 is critical and, therefore, estimative calculations of the Radio Frequency (RF) power available to the ASIC and back to the receiver are presented below. Typical values are taken from the literature [12] and the uncertainty may be up to 3 decibels (dB).

Table 2 Estimation of power budget for transponder's ASIC

		Observations/Comments
Transmitter Power	+33 dBm	This is a conservative value of 2W based on Table 1
Reader Antenna Directional Gain	+5 dBi	The gain for maximum directivity may be higher. This figure suggests operations within -3 dB beamwidth.
Cable and mismatch losses	-2 dB	Realistic values between transmitter and antenna
Reader's Antenna Circular Polarization Loss	-3 dB	This implementation mitigates tag's orientation in the field.
Free Space Transmission Loss	-40 dB	Based on 2.6 m typical range and 910 MHz
Average power loss due to reader's ASK modulation	-3 dB	This loss occurs during reader's command mode
Transponder Antenna Gain	+1 dBi	It is assumed a good impedance match between antenna and ASIC
Power available to ASIC	-9 dBm	Algebraic summation of the above values
Required ASIC input power	> -13 dBm	Specification available in data sheet [9]
Power Available - Required	4 dB	Estimated margin for ASIC operations

As can be seen from Table 2, there various gains and losses are added and subtracted to/from transmitter output and the final result estimates a 4 dB margin available for power to the ASIC's input.

Table 3 Estimation of power budget for reader's receiver

		Observations/Comments
Reflected Wave Power	-9 dBm	This value corresponds to the lowest level of modulated signal
Free Space Loss	-40 dB	Based on 2.6 m typical range and 910 MHz
Reader Antenna Directional Gain	+5 dBi	The gain for maximum directivity may be higher. This figure suggests operations within -3 dB beamwidth.
Cable and mismatch losses	-2 dB	Realistic values between transmitter and antenna
Reader Antenna Circular Polarization Loss	-3 dB	This implementation mitigates tag's orientation in the field.
SNR required for demodulation	-15 dB	This figure covers a wide range of modulation types
ASK sideband level	-6 dBc	The 100% ASK modulation by the tag has 25% power on each sideband. That has the information for the reader.
Power available to receiver	-70 dBm	Algebraic summation of the above values
Receiver sensitivity	-90 dBm	Specification available in data sheet [15]
Power Available - Sensitivity	20 dB	Estimated margin for receiver operations

As can be seen from Table 3, there various gains and losses are added and subtracted to/from reflected wave power and the final result estimates a 20 dB margin available for power to the input of the receiver.

It is concluded that the system design is critical for providing power to the ASIC.

1.1.4 Real Environment Operations

The wave transmitted by the reader is also reflected by other surfaces in the vicinity of a transponder. These reflected waves will create multipath interferences at the transponder. The result may be described as a spatial periodic cancellation and amplification of the signal's power.

As a result, the power available at the transponder is a function of the three-dimensional (3D) location in a real environment. In normal situations, the field power variations are found typically 5 dB at ranges around 2 m and as high as 10 dB at ranges around 3 m [1]. This variation is to be accounted in an actual design for a link margin.

1.2 *Communication Protocol for UHF RFID*

The **EPC™ Radio-Frequency Identity Protocols, Class-1 Generation-2 UHF RFID, Protocol for Communications** [2] specifies how the reader communicates with the transponder in 860 to 960 MHz frequency band. The following sections present the most important concepts defined in this standard, such as: frequencies and channel occupancy; reader modulation; tag modulation; data encoding; data rate and bandwidth; data integrity.

This international standard improved the performance, efficiency and capacity of RFID systems and the design using it can achieve the followings [3]:

- Trouble-free operation of multiple readers and multiple RFID applications
- Increased operational speed
- Backscatter options – provides the flexibility to maximize reader performance in ‘noisy’ environments
- Improved tag memory and programmability
- More robust tag communication design
- Enhanced security – increased password length provides better protection against

unauthorized access to tag data and functions (such as the 'kill' command to permanently deactivate a tag)

This protocol was implemented by various manufacturers in their latest ASIC designs. At present time the unique IDs are using 96-bits. The expansion to 128-bits IDs is predicted in the future and the present protocol will allow the transition.

The reader initiates the communications, starting with the first message called "preamble". This is a message containing synchronization and information bits for the transponder.

1.2.1 Frequencies and Channel Occupancy

The readers "talk first" and act as "master" of the RFID system, meaning that the tags always respond to reader's interrogation. During tag's response the readers transmit only a continuous wave (CW).

Communications are half-duplex, meaning that interrogators and tags do not transmit their messages at the same time. The tags transmit by modulating the CW received from the reader.

In North America there are 50 channels of 500 kHz each for a total bandwidth of 25 MHz.

In Europe the number of channels is reduced to 10 with 200 kHz each for a total bandwidth of 2 MHz. The spectral mask limits the data transfer rate from 1500 reads/sec in North America to 500 reads/sec in Europe, Japan [11].

Readers certified for operation in single and/or multiple interrogator environments must meet local regulations for out-of-channel and out-of-band spurious radio-frequency emissions.

The protocol specifies that a channel may be used for a limited time and a reader cannot

monopolize it. In order to satisfy this requirement, there are two main ways to operate multiple readers in the same area: using “duty cycle” or “listen before talk”. The Frequency Hopping Spread Spectrum (FHSS) is the widely favored standard. Using FHSS, the readers have inherent delays while waiting for channel availability.

1.2.2 Reader Modulation and Data Encoding

A reader communicates with transponders by modulating an RF carrier with Double Side Band-Amplitude Shift Keying (DSB-ASK), Single Side Band-Amplitude Shift Keying (SSB-ASK) or Phase Reversal- Amplitude Shift Keying (PR-ASK).

The data from reader to tags is encoded using Pulse Interval Encoding (PIE) symbols, presented below.

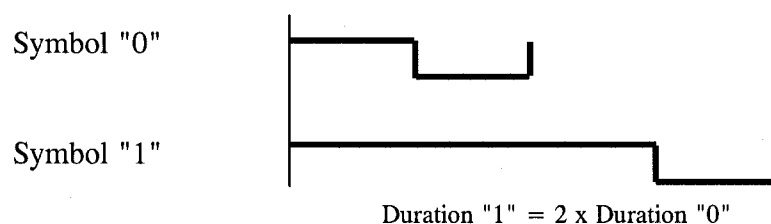


Figure 2 Pulse Interval Encoding symbols

The Figure 2 explains the relationship between PIE encoding and the modulation of the carrier. The higher level of each symbol represents maximum amplitude of transmitted CW and the lower level of each symbol represents attenuated amplitude of transmitted CW. The modulation depth is specified to be approximate 90%.

The PIE encoding has the advantage of increased average power due to signaling with short transitions to the low amplitude level. In this way, the power available to the tag is maximized when the reader is in “talk” mode.

1.2.3 Tag Modulation and Data Encoding

Tags modulate the CW from the reader using Amplitude Shift Keying (ASK) and/or Phase Shift Keying (PSK). The modulation type is predetermined by the ASICs hardware design [1] and will not be addressed here. Readers should be capable of demodulating either type.

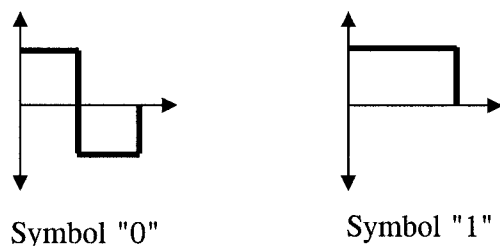


Figure 3 FM0 (Bi-Phase Space) symbols

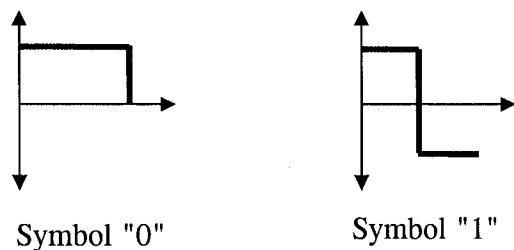


Figure 4 Miller symbols

Figures 3 and 4 illustrate data encoding from tag to reader, using Bi-Phase Space (FM0) or Miller symbols. As seen in both figures, the phase is changed at the boundary of each symbol, and the receiver (in the reader) can reconstruct them easier compared with other types of encoding.

The tags should be capable of using both FM0 and Miller symbols. The reader can change the encoding and/or the data rate of the transponder using commands contained in the preamble message.

1.2.4 Data Rate and Bandwidth

The duration of "0" symbol is the reference time interval for Reader-to-Tag signaling. The readers communicate with a "0" symbol rate selected between 40 kHz, 80 kHz or 160 kHz. For example: a standard 40 kHz symbol rate takes 80 kHz of fundamental bandwidth. In order to ensure a non-distorted waveform for accurate decoding, the third harmonic (at 240 kHz) should pass through the baseband output filter at the transmitter [14]. This requires a minimum of 240 kHz (plus a buffer) for a channel bandwidth.

Similarly, various tag data rates determine 40 kHz to 640 kHz occupied bandwidth. With higher modulation frequencies, the tag's reflected wave is placed outside of the transmitter's channel and sometimes outside the approved frequency band. This situation is presented in the figure below.

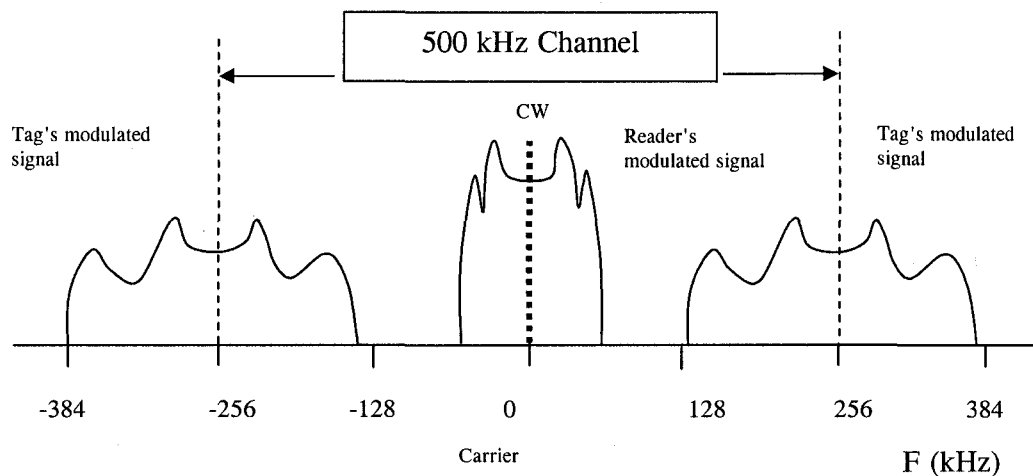


Figure 5 Subcarrier spectral allocation for 902 to 928 MHz band

The Figure 5 illustrates the occupied bandwidth and the relationship between the modulated signals from the reader and from the transponder. In this case, the reader has 40 kHz data rate and the transponder has between 128 and 640 kHz data rate. Higher modulation frequencies for transponder's communications have the following advantages and

disadvantages [14]:

- The communications are typically more robust as the reader decodes signals further away from the carrier
- Higher tag data rates facilitate shorter tag messages and less risk of collisions with other tags
- Tag emissions are not substantial enough to produce prohibited power levels outside the reader's channel and do not exceed regulations for spurious signals
- Reader placement and interrogation zone must account for the interference with other systems using the same frequency band and operating in proximity

1.2.5 Data Integrity

Messages from reader and transponder are verified by using the classic Cyclic Redundancy Check (CRC) procedures. The EPC Gen2 standard uses CRC-16.

Anti-collision algorithms are implemented to guarantee access to multiple tags in the field of one reader. The ALOHA procedure and the variants of Slotted ALOHA and Dynamic Slotted-ALOHA use variable time delays for tag response. The implementation of the EPC Gen2 standard uses a pseudo-random number generator in the ASIC that is activated by a specific reader command.

1.3 *Transponder Parameters Affecting System Performance*

The transponder is fabricated by attaching the ASIC on a UHF antenna. Most UHF antennas are a design compromise between conflicting requirements. The size, shape, sensitivity of operations in proximity to different materials and cost are all important trade-offs in an overall design. There is no one 'right' transponder for all applications and, therefore, this field of RF design is open for innovative ideas.

The well known principle for tag's antenna design is to conjugate-match its output impedance to the ASIC's input complex impedance in order to maximize the power transfer.

The ASIC's complex impedance is known from the datasheet or measurement. Typically the impedance is expressed as parallel RC. The resistance and the capacitance are variable in the 860MHz to 960MHz frequency range and in the -9dBm to -14dBm power range.

For worldwide application, a UHF tag must be capable to operate from 860 MHz to 960 MHz frequency range to meet all regulations. This requirement has a major impact in transponder antenna design and will trade-off with other parameters that are affecting the performance.

The antenna orientation issues are usually mitigated by the setup of the reader antenna. For optimal performance, the transponder manufacturer formulates recommendations for attachment on the specific product. In addition, restrictions of relative motion speed of the transponder in the field of the reader are specified.

1.3.1 Antenna Size and Shape

Tag form and size must be such that it can be embedded or attached to objects such as cardboard boxes, airline baggage strips, identification cards or fit inside a printed label. Therefore, from application point of view, it is generally desired to have small tags. On the other hand, large tag antennas provide more power to the ASIC and larger scatter aperture which reflects more signal back to the reader. In other words, maximizing antenna gain asks for large tags. These two conflicting requirements need to be balanced in a design.

Size and shape play an important role in antenna complex impedance. An adjustment of

the impedance by modifying the antenna size is not practical due to the fact that both resistance and reactance can change at the same time. As a result, it is preferable to adjust the impedance by changing the shape.

The ASIC's impedance is typically resistive-capacitive and, therefore, to achieve a conjugate match an inductive antenna is required. The restrictions on the size of tag's antenna require that the matching network to be embedded into the antenna layout. The desired changes of inductive or resistive characteristics are done by modifying the length and location of various antenna parameters. These parameters are specific to the chosen construction format or shape of the antenna.

Typical antenna sizes are about a quarter wavelength, i.e. $\lambda/4$. The antenna directivity on the main direction is typically between 1.5 dBi and 1.9 dBi [10]. For reference, the directivity of a standard $\frac{1}{2}$ wavelength dipole is 2.14 dBi.

Antenna design is the pivotal stage of transponder design and determines the overall performance for a specific set of given requirements.

1.3.2 Fabrication Materials and Process

Antenna construction requires good electrical conductor and substrate:

- Conductor examples: copper, conductive ink
- Substrate examples: high density polyethylene (HDPE) or polypropylene (PP)

The substrate has three main design parameters: dielectric constant (ϵ_r) and loss tangent ($\tan \delta$) and thickness. High values of dielectric constant reduce the effective wavelength, lower the resonant frequency and narrow the bandwidth. High values of $\tan \delta$ reduce the radiated power and increase bandwidth. A thick substrate accentuates the effects of above mentioned parameters.

One of the reliable assembly methods for connecting the ASIC to the antenna is using conductive adhesive, conferring low temperature process and low cost. However, in practice, to prevent oxidation, the contact pads on the copper or aluminum antenna must be plated over with nickel-gold, nickel-palladium or nickel-silver, just like the contact bumps on the ASICs. These additional processes do increase costs.

Alternatively, the antenna traces may be printed or otherwise deposited with precious metal ink using the traditional thin or thick-film process. One of the drawbacks of this approach is the variation in conductivity when longer fine traces are printed. Variation of conductivity also induces variation in read-write distance capability. Thus, thick film process tends to be used only for the 2.45 GHz and the 915 MHz RFID tags that have simpler geometry and wider traces.

1.3.3 Proximity to Objects

Antenna electromagnetic properties may be altered when objects are placed in close proximity:

- High dielectric constant objects with high loss (e.g. plastics; water) can detune the tag and reduce radiation efficiency
- Conductive objects cause large increase in antenna radiation resistance and prevent efficient power transfer

Tag antenna can be designed or tuned for optimum performance on a specified object.

1.3.4 Tag's Orientation vs. Reader's Antenna

Efficient power transfer between a reader and a tag is also determined by the polarizations of reader's and tag's antennas. The relative orientation is critical if both reader and tag have linearly polarized antennas.

The widely implemented solution to mitigate the random orientation of the transponder is to have circular polarization of the reader's antenna. It is known that the trade-off for using this type of antenna is a 3 dB loss in power compared with a linearly polarized antenna.

Some transponders also have circular polarization [24]. They use two dipoles perpendicular on each other. The 90 deg. out-of-phase is produced by a $\lambda/4$ delay line attached to the feed of the two dipoles.

Recent readers have four RF input/output ports controlled sequentially. The four antennas attached to these ports are placed in such a way to illuminate the field from different angles and/or have orthogonal directions. This way, the reading zone is configured to minimize the possible loss of communication with transponders, indifferent of their orientation.

1.3.5 Deformation

Tags are often designed for flat surfaces. Flexible tags are then developed at large scale and at very low costs. When these tags are attached to non-flat surfaces, the deformation changes the radiation properties.

Performance degradation due to deformation of the geometry of antenna is causing impedance change (mismatch) or de-tuning. In fact, the antenna is offset for different resonant frequency and matching impedance. This undesired effect is mitigated by proper usage/application of the transponder to products.

1.3.6 Density and Relative Motion Speed

Close proximity to other transponders and objects placed in the line-of-site of transponder with the reader affect the transmission between reader and tag. In other words, degradation effects occur with a high density and a specific distribution of tags in the reader' field.

The relative motion speed between tag and reader also affects directly communications with high speed Doppler shift. In case of multipath interference, the relative motion may benefit sometimes the identification of the total tag population.

2 REVIEW OF ANTENNA THEORY

2.1 Fundamental Parameters of Antennas

The performance of an antenna is described with various parameters [4]. The relevant parameters are presented below.

2.1.1 Radiation Pattern

An antenna does not radiate energy uniformly in all directions. Such characteristic of the spatial variation of the power density along a constant radius is called a *radiation power pattern*. In most cases, the radiation pattern is determined in the far-field region and is represented as a function of the directional coordinates [4].

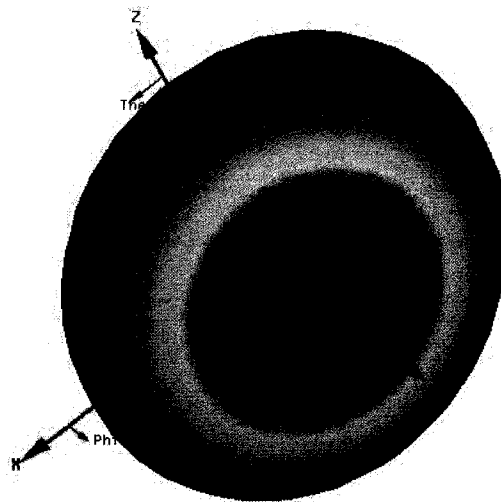


Figure 6 Radiation pattern of a dipole

As example, the Figure 6 illustrates the radiation pattern of a dipole antenna.

The space surrounding an antenna is usually subdivided into three regions:

- (a) reactive near-field $0 < r < 0.62\sqrt{D^3/\lambda}$
 (b) radiating near-field (Fresnel) $0.62\sqrt{D^3/\lambda} < r < 2D^2/\lambda$
 (c) far-field (Fraunhofer) $2D^2/\lambda < r < \infty$

where r is the radius of the field, D is the largest dimension of the antenna and λ is the wavelength.

As the distance is varied from the reactive near field to the far field, the amplitude pattern of an antenna changes in shape because of variations of these fields.

The *time average Poynting vector* can be written as $W_{av} = \frac{1}{2} \text{Re}[\mathbf{E} \times \mathbf{H}^*]$ (W/m²) and represents the real part of the instantaneous Poynting vector. This quantity is the average power density associated with the electromagnetic fields of an antenna in its far-field region.

The imaginary part of the instantaneous Poynting vector represents the reactive (stored) power density.

The total *average power* radiated by an antenna can be written as $P_{rad} = P_{av} = \oint_S W_{av} \cdot ds$

Beamwidth is the angular separation between two identical points on opposite side of the pattern maximum. In an antenna pattern, there are a number of beamwidths. One of the most widely used beamwidths is the *Half-Power Beamwidth (HPBW)*, which is the angle between the two directions in which the radiation intensity is one-half value of the maximum beam.

The solid angle $d\Omega$ of a sphere can be written as $d\Omega = dA/r^2 = \sin\theta \cdot d\theta \cdot d\phi$ where θ is the elevation and ϕ is the azimuth of a classic spherical coordinate system.

Radiation intensity in a given direction is defined as the power radiated from an antenna per unit solid angle. In mathematical form it can be expressed as $U = r^2 \cdot W_{av}$

Therefore, another expression for the radiated power can be written as

$$P_{rad} = \iint_{\Omega} U d\Omega = \int_0^{2\pi} \int_0^{\pi} U \sin\theta d\theta d\phi$$

This above expression will allow the introduction of the radiation intensity for an *isotropic*

source, which is uniform in all directions.

$$U_0 = \frac{P_{rad}}{4\pi}$$

In the case of the dipole operating in air, placed on the vertical axis and centered in the origin, the radiation intensity is found to be

$$U = r^2 W_{av} = \eta \frac{|I_0|^2}{8\pi^2} \left[\frac{\cos\left(\frac{kl}{2} \cos\theta\right) - \cos\left(\frac{kl}{2}\right)}{\sin\theta} \right]^2$$

where l is the length of the dipole, $k = 2\pi/\lambda$ is the wave number in air, $\eta = 377$ ohm is the intrinsic impedance of the air, I_0 is the amplitude of current in the antenna with sinusoidal distribution, θ is the elevation measured from the vertical.

Usually the power pattern is normalized with respect to his maximum value and plotted on a logarithmic scale (dB).

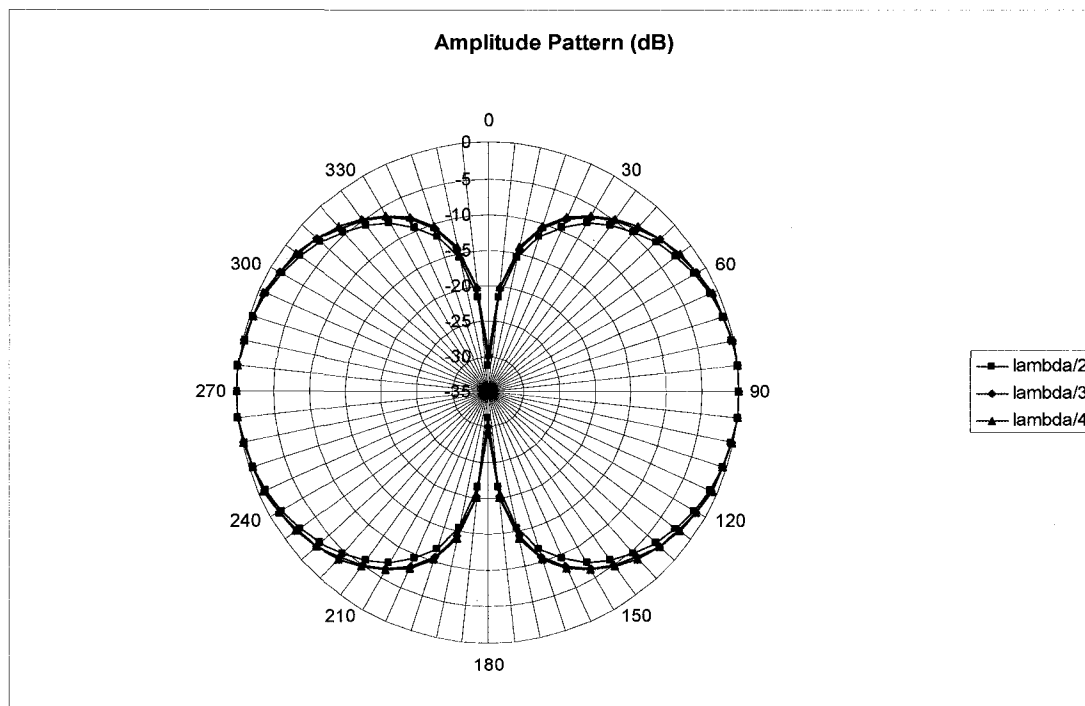


Figure 7 Radiation patterns for a thin small dipole with different lengths

Figure 7 presents the radiation patterns for three dipoles with lengths of $l = \lambda/4$, $\lambda/3$ and $\lambda/2$, respectively, calculated with the formula for U above.

Directivity of an antenna is defined as the ratio of the radiation intensity in a given direction to that of an isotropic source. In mathematical form it can be written as

$$D = \frac{U}{U_0} = \frac{4\pi U}{P_{\text{rad}}}$$

and is dimensionless. The directivity is a function of two variables: θ (elevation) and ϕ (azimuth).

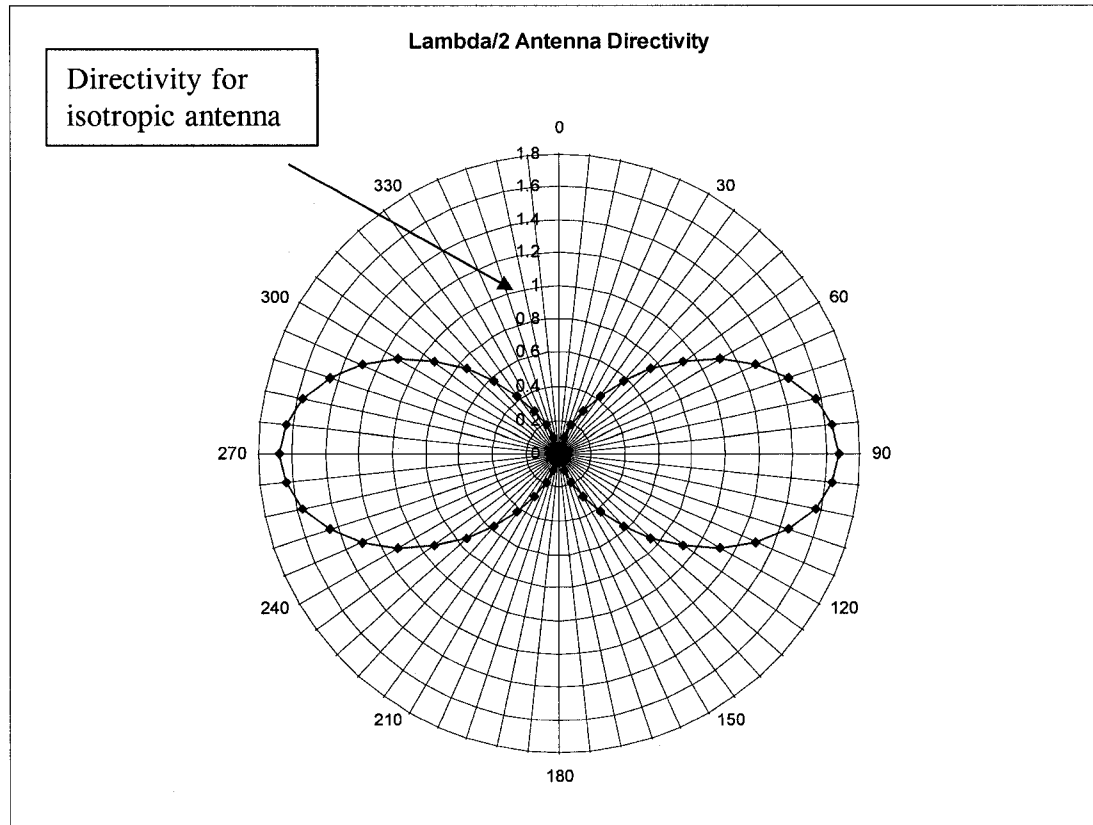


Figure 8 Directivity pattern of a $\lambda/2$ dipole in the elevation plane

Figure 8 illustrates graphical representation of directivity for a $\lambda/2$ dipole in a two-dimensional plot. The maximum directivity linear value is 1.67, equivalent with 2.14 dBi.

2.1.2 Antenna Efficiency

The total antenna efficiency is used to take into account losses at the input terminals and within the structure of an antenna [4].

$$e_0 = e_r e_{cd} = e_{cd}(1 - |\Gamma|^2)$$

The first term e_{cd} represents the efficiency due to conduction and dielectric losses.

$e_{cd} = \frac{P_{rad}}{P_{in}}$ This term is very difficult to compute and it is usually determined experimentally.

The second term $1 - |\Gamma|^2$ represents the power transmission coefficient due to the mismatch between the impedances of transmission line (Z_0) and the antenna (Z_A), where Γ is the reflection coefficient. $\Gamma = \frac{Z_A - Z_0}{Z_A + Z_0}$

2.1.3 Gain

The gain of the antenna is closely related to the directivity and it is a measure that takes into account the efficiency of the antenna as well as its directional capabilities [4]. The gain is defined as $G = e_{cd} \cdot D$. The maximum gain is found on the direction of maximum directivity.

2.1.4 Polarization

Polarization of an antenna in a given direction is defined as the polarization of the wave transmitted (radiated) by the antenna [4]. At any local point in the far field, this is defined as the loci of the tip of the electric field vector, whose direction of propagation is in the radial direction from the antenna. Polarization may be classified as linear or elliptical (circular is a particular elliptical case).

If the polarization of transmit and receive antennas are not matched, a polarization loss is created. The *polarization loss factor* for linearly polarized antennas is found as $\cos^2 \psi$ where ψ is the angle between the vectors of electric field intensity of the waves by a transmit and receive antennas, respectively.

2.1.5 Bandwidth

The bandwidth is considered the range of frequencies for which the pattern and the impedance are within an acceptable limit from the shape and values determined at the central frequency [4].

There is a distinction made between pattern bandwidth and impedance bandwidth because these two characteristics do not vary in the same manner. For example, the radiation pattern of a linear dipole with overall length less than a half-wavelength ($l < \lambda/2$) is insensitive to frequency, except that the impedance is [4].

For this project, the requested bandwidth is calculated as function of maximum, minimum and central frequencies, as follows:

$$\frac{(F_{\max} - F_{\min})}{F_c} = \frac{(960 - 860)}{910} \cong 11\%$$

Nevertheless, gain, beamwidth, polarization, impedance and bandwidth are related.

2.1.6 Input Impedance

The impedance presented by an antenna at its terminals is the ratio of the voltage to current or the ratio of the appropriate components of the electric to magnetic fields [4]. The mathematical expression is: $Z_A = (R_r + R_L) + jX_A$ where the complex impedance = resistance (due to radiation and loss) + j * reactance (due to energy stored in the near field of the antenna).

Using Thevenin equivalent circuit of an antenna connected to a load (or generator) the captured (total) power, reradiated (scattered) power and power delivered to the load can be calculated as functions of impedance. These expressions are not used directly in this project and, therefore, not presented.

The most important conclusions are enumerated below:

- An antenna operating in receiving mode and properly matched, i.e. under maximum power transfer, has half of the power delivered to the load and the other half scattered back or reradiated.
- The input impedance of an antenna is generally a function of frequency. Thus the antenna will be matched only within a frequency bandwidth.
- The input impedance of an antenna depends on many factors including its geometry, its method of excitation, and its proximity to surrounding objects. Because of their complex geometries, only a limited number of practical antennas can be studied with analytical formulations.

The resistance due to radiation for a dipole of length l is usually computed by numerical integration. The current distribution and general impedance, especially of wire-type antennas, are functions of the radius of the wire and feed gap spacing and can be easily taken into account by using advanced computational methods and numerical techniques. For the $\lambda/2$ dipole at resonant frequency, the input impedance is found to be $Z_{in} = 73 + j42.5$ (ohms)

2.1.7 Antenna Equivalent Areas

The *effective area (aperture)* of an antenna in a given direction is defined as the ratio of the available power at the terminals of a receiving antenna to the power flux density of a plane wave incident on the antenna from that direction [4].

Mathematically, the effective area is written as $A_e = P_T/W_i$ where P_T is the power delivered to the load and W_i is the power density of incident wave.

In similar way, *the scattered (reradiated) area* and *the loss (conduction and dielectric) area*

are introduced. Under matched and lossless conditions, the maximum effective area (A_{em}) has the same value as the scattered area (A_s) and maximum power transfer occurs.

For aperture type antennas (waveguides, horns and reflectors) the maximum effective area does not exceed the physical area. However, for wire antennas, the maximum effective area may be thousands of times larger than the physical area. For the $\lambda/2$ dipole $A_{em} \cong 0.13 \cdot \lambda^2$

The maximum effective aperture (A_{em}) of any antenna is found to relate to its maximum directivity (D_0) with $A_{em} = \frac{\lambda^2}{4\pi} D_0$

Including antenna efficiency and the polarization loss, the expression becomes

$$A_{em} = e_{cd} (1 - |\Gamma|^2) \frac{\lambda^2}{4\pi} D_0 \cdot \cos^2 \psi$$

2.1.8 Friis Transmission Equation

Friis equation relates the power received by an antenna to the power transmitted by another antenna, with a distance $R > 2l^2/\lambda$ between the two antennas, where l is the largest dimension of either antenna [4].

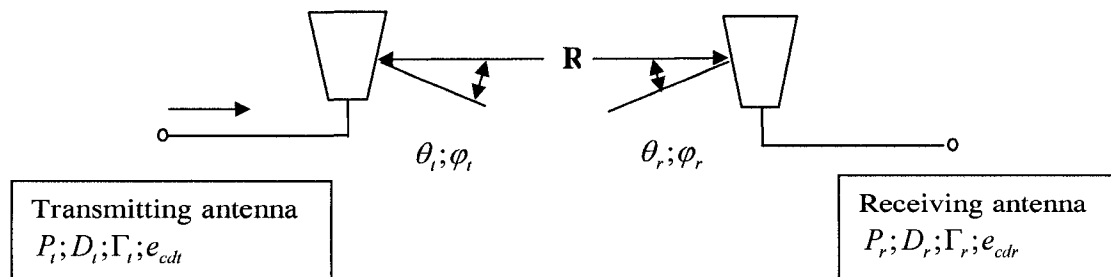


Figure 9 Transmitting and receiving antennas for Friis transmission equation

Considering the scenario shown in Figure 9, where one antenna is transmitting and a second antenna is receiving, the Friis transmission equation can be written as:

$$\frac{P_r}{P_t} = \left(\frac{\lambda}{4\pi R} \right)^2 \cdot e_{cdt} (1 - |\Gamma_t|^2) D_t(\theta_t, \varphi_t) \cdot e_{cdr} (1 - |\Gamma_r|^2) D_r(\theta_r, \varphi_r) \cdot \cos^2 \psi \quad \text{where transmitting}$$

antenna has the following parameters: P_t is the input power at antenna terminals, D_t is the directivity, Γ_t is the reflection coefficient at terminals, e_{cdt} is the efficiency, θ_t and φ_t are the elevation and azimuth angles of the associated polar coordinates system. The $P_r; D_r; \Gamma_r; e_{cdr}; \theta_r; \varphi_r$ are similar parameters associated with the receiving antenna. $\cos^2 \psi$

is the polarization loss factor between the two antennas. The term $\left(\frac{\lambda}{4\pi R} \right)^2$ is often called the *free-space loss factor*, and it takes into account the losses due to the spherical spreading of the energy of a wave in space.

2.1.9 Antenna Radar Cross Section

The radar cross section, usually referred to as RCS, is a far-field parameter, which is used to characterize the scattering properties of a radar target [4].

In general, the RCS of a target is a function of the polarization of the incident wave, the angle of incidence, the angle of observation, the geometry of the target, the electrical properties of the target, and the frequency of operation. The units of RCS of three-dimensional targets are meters squared or, for normalized values, decibels per squared meter (dBsm).

For a target, there is *monostatic* or *backscattering RCS* when the transmitter and receiver are at the same location. For simplicity, if the antennas are identical and are polarization-matched the total radar cross section of the antenna for backscattering can be written as

$$\sigma = \frac{\lambda_0^2}{4\pi} G_0^2 |A - \Gamma^*|^2 \quad \text{where} \quad \Gamma^* = \frac{Z_L - Z_A^*}{Z_L + Z_A^*} \quad \text{is the conjugate-matched reflection}$$

coefficient (or Kurokawa's power wave reflection coefficient), G_0 is the gain for maximum directivity and A is a complex parameter independent of the load.

If the antenna is a thin dipole, then $A \cong 1$ and the expression reduces to

$$\sigma \cong \frac{\lambda_0^2}{4\pi} G_0^2 |1 - \Gamma^*|^2$$

For the $\lambda/2$ dipole that is short-circuited ($Z_L = 0$) $\sigma \cong 0.86 \cdot \lambda^2$ is obtained. It is important to be mentioned that the short-circuit RCS of an antenna is larger than the RCS of the same antenna matched to a load.

2.2 Broadband Dipoles

The successful design of the transponder antenna required a bandwidth of 860 to 960 MHz which is difficult to achieve with a simple dipole. As a result, variations of dipoles have been developed.

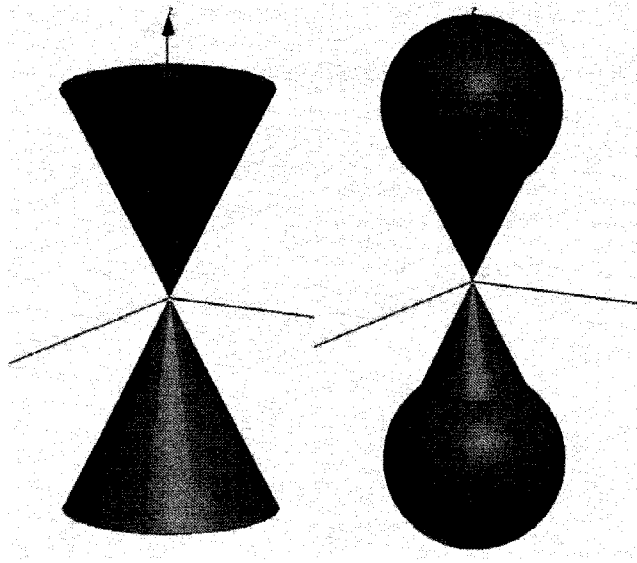


Figure 10 Biconical and tapered dipole antenna geometries

Figure 10 shows two broadband typical structures, the biconical and the tapered dipole antennas. The biconical antenna has less matching efficiency compared with the tapered one, but is easier and economical for practical implementation. When the angle of the cone increases, the variation of impedance decreases across the frequency band [4] and this will lead to a broadband antenna.

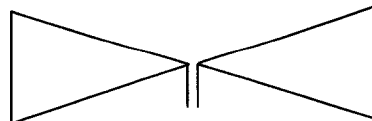


Figure 11 Bow-tie antenna

Figure 11 shows the geometrical approximation to the solid or shell biconical antenna, and is called bow-tie antenna. This antenna is popular for easy fabrication, however, does not exhibit as large broadband characteristics as the corresponding solid biconical antenna.

Other antenna structures are thick dipole, folded dipole, dielectric coated antennas, and all have advantages and disadvantages in respect with a specific application. In general, as a practical technique, bandwidth can be increased by enlarging the area associated with the ends of the antenna.

2.3 Peak Power Gain Measurement and Sources of Error

Peak power is associated with the direction of maximum directivity. The two antennas used are separated so that far-field conditions are satisfied, as mentioned in section 1.1.2.

There are two general methods applied for measurement: *absolute-gain measurements* and *gain-transfer measurements* [13]. In this project both methods are used.

Absolute-gain measurements are based upon the Friis transmission formula. The procedure requires an optimal calibration of the coupling network between the source/load and the transmitting/receiving antennas so that the power measured at the transmit/receive test point is accurate.

The gain-transfer method, which is also referred to as the *gain-comparison method*, is the most commonly employed method for power-gain measurements. This method requires the use of an antenna standard for which the gain is known and compared with the antenna under test. The two widely accepted standard antennas are the dipole and the pyramidal horn.

For circularly polarized antennas gain measurement, linearly polarized standard antennas

can be used to measure successively two orthogonal polarizations gains. Calculation of total gain is using the following formula: $(G_T)_{dB} = 10 \log (G_{TV} + G_{TH})$ where G_T is the total power gain; G_{TV} and G_{TH} are the partial power gains measured with respect to vertical and horizontal linear polarizations. The uncertainty of measurement can be between -0.915 dB and 0.828 dB if the cross polarization of the linearly polarized antenna is 20 dB [4].

Multiple factors are contributing as sources of error for gain measurement. The most prominent are the impedance mismatch between generator and transmitting antenna and receiving antenna and load.

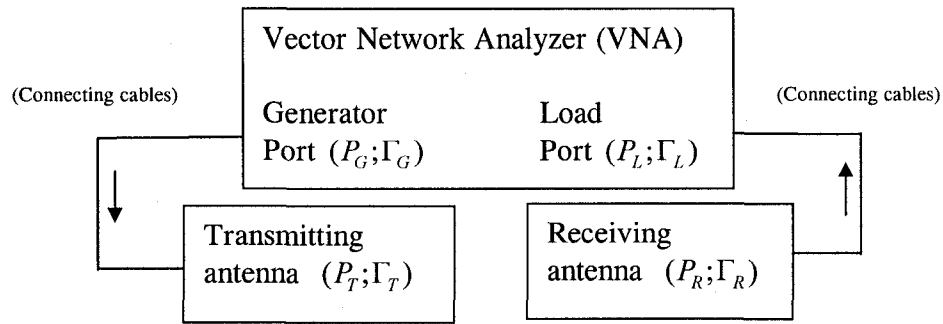


Figure 12 Setup for peak power gain measurement

Figure 12 shows a Vector Network Analyzer (VNA) used for gain measurement in this project. The power transfer between generator port and transmitting antenna can be written as: $P_T = P_G \cdot M_1$. The power transfer between receiving antenna and load port can be written as: $P_L = P_R \cdot M_2$. P_G , P_T , P_R and P_L are introduced in the Figure 12 and represent power in/out of respective ports. The expressions for M_1 and M_2 are:

$$M_1 = \frac{(1 - |\Gamma_G|^2)(1 - |\Gamma_T|^2)}{|1 - \Gamma_G \Gamma_T|^2} \quad \text{and} \quad M_2 = \frac{(1 - |\Gamma_R|^2)(1 - |\Gamma_L|^2)}{|1 - \Gamma_R \Gamma_L|^2}$$

where Γ are reflection coefficients of different ports shown in Figure 12 and calculated with respect to the characteristic impedance of the transmission lines [13]. In this setup the

characteristic impedance of connecting cables is 50 ohm.

The terms $1 - |\Gamma|^2$ are power transmission coefficients and can be calculated using the measured magnitudes of the reflection coefficients.

The terms $(1 - \Gamma_R \Gamma_L)^2$ and $(1 - \Gamma_G \Gamma_T)^2$ seen in the formulas of M_1 and M_2 contribute to measurement uncertainty. This is explained by the unknown phase relationship between the reflection coefficients Γ , which are complex numbers, at the time when the actual measurement is done. The overall measurement uncertainty M is expressed as an interval of possible values, where the minimum and the maximum values are calculated using the following formula:

$$M = \frac{(1 \mp |\Gamma_G| \cdot |\Gamma_L|)^2}{(1 \pm |\Gamma_R| \cdot |\Gamma_L|)^2 (1 \pm |\Gamma_G| \cdot |\Gamma_T|)^2} \quad \text{where } (1 \mp |\Gamma_G| \cdot |\Gamma_L|)^2 \text{ is the transmission uncertainty}$$

of the VNA calibration, $(1 \pm |\Gamma_R| \cdot |\Gamma_L|)^2$ is the transmission uncertainty between receiving antenna and the load port and $(1 \pm |\Gamma_G| \cdot |\Gamma_T|)^2$ is the transmission uncertainty between generator port and transmitting antenna.

3 UHF RFID TRANSPONDER ANTENNA DESIGN

Requirement: transponder operations over 860 to 960 MHz frequency band with a range over 2 m.

The design method applied in this project is summarized below:

1. Analysis of design inputs: antenna size and shape; fabrication materials and cost; objects in vicinity.
2. ASIC impedance measurement. The impedance is usually given by the ASIC manufacturer in the datasheet and measured for verification purposes.
3. Antenna design, parametric study and optimization; performance estimation.
4. Fabrication and measurement of prototypes. Iterations of the last two steps may be required until the performance meets design requirements.

The study and optimization of the antenna is done by using Ansoft HFSS™ software package, which is based on Finite Element Method (FEM). The evaluation of the prototypes is based on measurements done inside the anechoic chamber in order to limit multipath interferences existent in a real environment.

3.1 *Analysis of Design Inputs*

The central frequency of 860 to 960 MHz frequency band is considered to be $f_c = 910\text{MHz}$ for convenience of calculations and measurements. The central wavelength is calculated as $\lambda = \frac{c}{f_c} = 329.67\text{mm}$.

The shape of the antenna for this design is a variation of a planar bow-tie. This is a logical choice based on considerations made in section 2.2 about increased bandwidth antenna geometries.

The size of the antenna is searched in the $\lambda/4 < l < \lambda/3$ interval. As a result, the 3 dB-beamwidth is in 78° to 87° interval [4] and the radiation pattern is similar with the ones presented in Figure 7. As mentioned in section 1.3.1 the antenna maximum directivity is typically between 1.5 dBi and 1.9 dBi [10].

The fabrication materials of choice for the transponder antenna are copper plated on FR4 substrate, used usually for printed circuit boards (PCB). This was based on availability of accurate PCB layout tools and prototype manufacturers. For FR4 substrate, the relative permittivity is $\epsilon_r = 4.4$ and the dielectric loss tangent is $\tan \delta = 0.02$. The substrate has 62 mil thickness (1.6 mm). The copper is plated with 1 oz/sq.in, equivalent with 0.034 mm thickness. Some advantages are mentioned:

- The inflexible substrate will prevent deformations
- The PCB is more reliable compared with conductive ink deposited on a high density polyethylene substrate.

These materials do not offer the best costs and may not be suitable for a large range of applications, except that are optimal for academic purposes.

The ASIC available for this project is RI-UHF-STRAP-08 from Texas Instruments (TI), that complies with EPCGlobal™ UHF Gen2 Standard.

Specifications important for this design are presented below:

- Maximum RF Exposure between 800 and 1000 MHz is 10 dBm.
- Typical reading sensitivity -13 dBm.
- Change in modulation of reflection coefficient $\Delta\Gamma > 0.2$.

The scope of this project does not include objects in near vicinity of the transponder. This ideal case will pose some challenges during the measurement and performance evaluation of the first prototype due to reflected power from the close reflective surfaces. Therefore, it is important to keep large reflective objects in the antenna far-field. The calculation of

far-field lower limit using the formula presented in section 2.1.1 (as $2l^2/\lambda$) with approximate antenna size of $l=\lambda/3 \approx 110$ mm, will result in a value of 73 mm.

The operation range of the transponders is expected to be maximal at central frequency, where the impedance matching is optimal. At both ends of the frequency range, the operations range must meet the requirement.

3.2 ASIC Impedance

3.2.1 Texas Instruments ASIC

This ASIC was the only available option for procurement at the time when the project was initiated. The search for different ASICs was extended to other manufacturers and, unfortunately, the purchase requests were not successful.

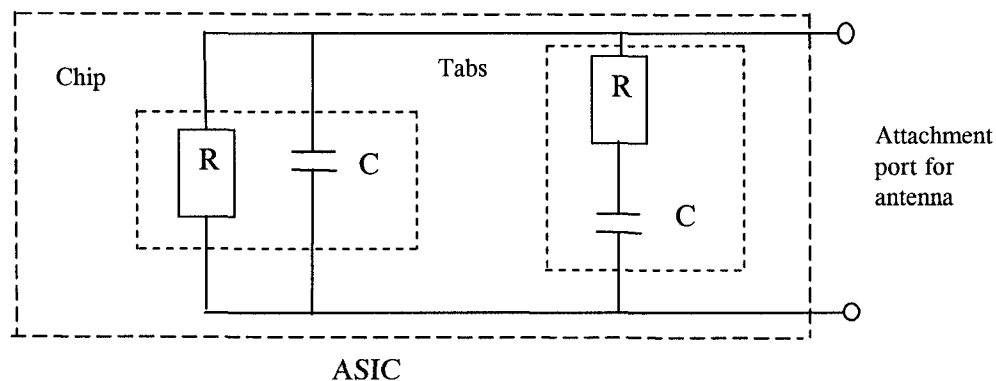


Figure 13 Internal configuration for ASIC's impedance

Figure 13 illustrates the internal configuration for ASIC's impedance. This contains the impedance of the chip in parallel with the impedance from the tabs. The tabs are providing the attachment port for transponder's antenna and their size of approximate 3 mm x 3 mm makes the transponder assembly process easier [9].

Table 4 Impedances of TI chip at different frequencies and power levels

Parallel Impedance	865 MHz	915 MHz	955 MHz
Resistance at -13 dBm	440 ohm	380 ohm	340 ohm
Capacitance at -13 dBm	2.8 pF	2.8 pF	2.8 pF
Resistance at -9 dBm	360 ohm	330 ohm	300 ohm
Capacitance at -9 dBm	2.7 pF	2.8 pF	2.9 pF

Table 4 presents detailed input impedance of TI chip [10]. It is noticeable that the chip input impedance is variable with frequency and input power level.

Standard equations are used to convert the chip impedance from a parallel to series configuration. The calculations were done using an Excel spreadsheet only for -13 dBm of input power level (see details in Appendix 1), and the results are summarized in the Table 5. The reactance's negative sign indicates the capacitive nature of the impedance.

Table 5 Series impedance for TI chip

Series Impedances at -13 dBm	865 MHz	910 MHz	955 MHz
Resistance	9.5 ohm	10 ohm	9.5 ohm
Reactance	-63.9 ohm	-60.8 ohm	-56.1 ohm

The impedance introduced by the tabs at mid band is approximately a 3.5 ohms resistor in series with a capacitor of 0.095 pF [10].

The calculations for total ASIC impedance, as shown in Figure 13, were done using an Excel spreadsheet only for -13 dBm of input power level (see details in Appendix 2), and the results are summarized in the Table 6.

Table 6 Series impedance for TI ASIC for -13 dBm input power level

ASIC Series Impedance	865 MHz	910 MHz	955 MHz
Resistance	8.9 ohm	9.4 ohm	9. ohm
Reactance	-61.9 ohm	-58.9 ohm	-54.5 ohm

The calculations for ASIC reflection coefficient were done using an Excel spreadsheet (see Appendix 3), and the impedance variation is plotted on the Smith Chart (courtesy of www.rfcafe.com) only for -13 dBm input power level.

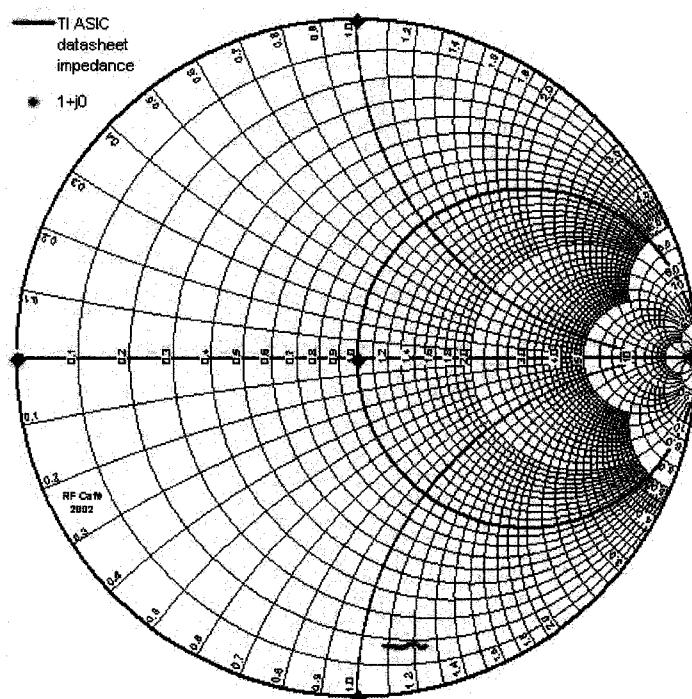


Figure 14 ASIC datasheet impedance variation on the Smith Chart

The impedance data available for -9 dBm input power level was not processed because the design will target optimal matching for the most unfavorable case (-13 dBm input power level). The operations are not affected with more power available at ASIC's input – even if the reflection coefficient is different by a small amount.

3.2.2 ASIC Impedance Measurement

The ASIC impedance measurement was performed to verify the datasheet values. The Vector Network Analyzer (VNA) AGILENT 8722ES available in the Wireless Laboratory at Dalhousie University was used for the measurement.

3.2.2.1 Setup and Calibration

The most accurate measurement of such impedance requires a complex setup called “Load Pull” and is described in [10]. However, many of the test components are unavailable for us to perform such a measurement. The use of the VNA is an acceptable alternative but will have less accuracy than Load Pull method.

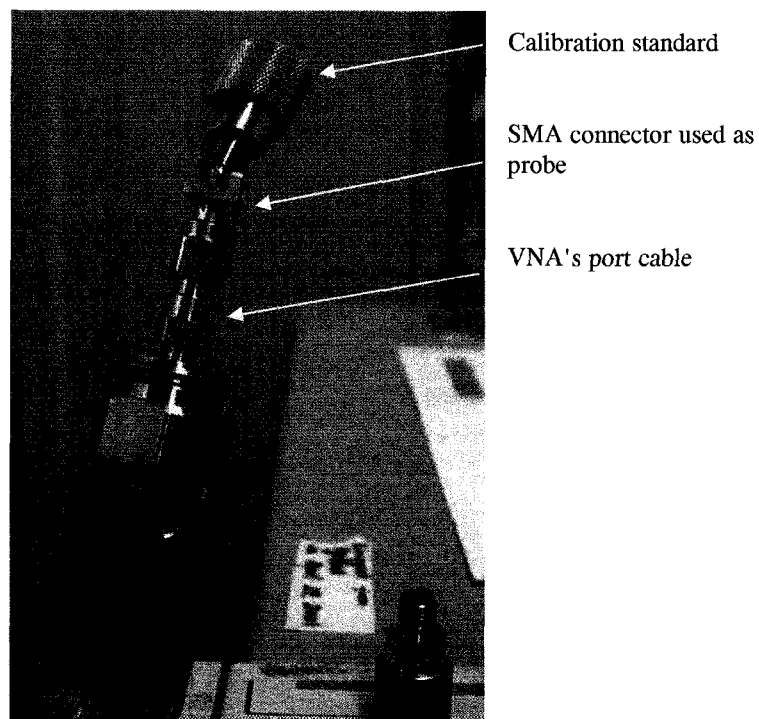


Figure 15 VNA's 1-Port calibration for impedance measurement

The Figure 15 illustrates how the VNA's calibration was done using the calibration

standards available in the 85052D Calibration Kit [also identified as 3.5 mm D]. The probe employed for the VNA measurement was a Sub Miniature version A (SMA) PCB connector attached to the VNA's port cable.

The main reason for the SMA probe was that the pins (center and ground) of the connector are rigid and can keep the impedance constant during the calibration and during the measurement. The special cable attached to VNA's port are flexible and are not expected to change phase and magnitude of the signal when are used within specified bend-radius.

In order to minimize the errors and obtain the best possible accuracy, the 1-Port full calibration of a VNA is carried out using the following parameters: frequency range set between 860 to 960 MHz; power output level set to -13 dBm; average factor set to 16. Verification of the calibration was done using Smith Chart view and standards with known impedance. The calibration data was saved in the instrument memory and was also used to measure prototype antennas impedance.

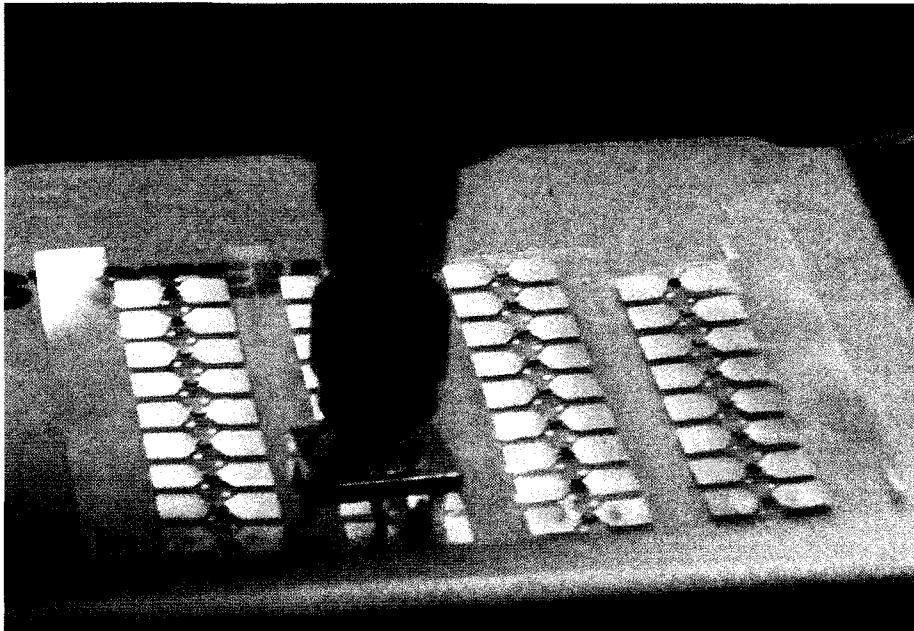


Figure 16 ASIC impedance measurement

Figure 16 presents the probing of the ASIC's for impedance measurement. The support was provided by a cardboard box. It was noticed that the material of the object supporting the ASIC during probing does change the impedance measurement. The amount is different in case of cardboard, wood, plastic or metal.

3.2.2.2 Measurement Results

Four ASICs were measured at five input power levels: -10; -11; -12; -13 and -14 dBm. The variation of the impedance with power level is analyzed for one ASIC. Appendix 4 contains impedance measurement data for one ASIC at five power levels. All other impedances show similar trend.

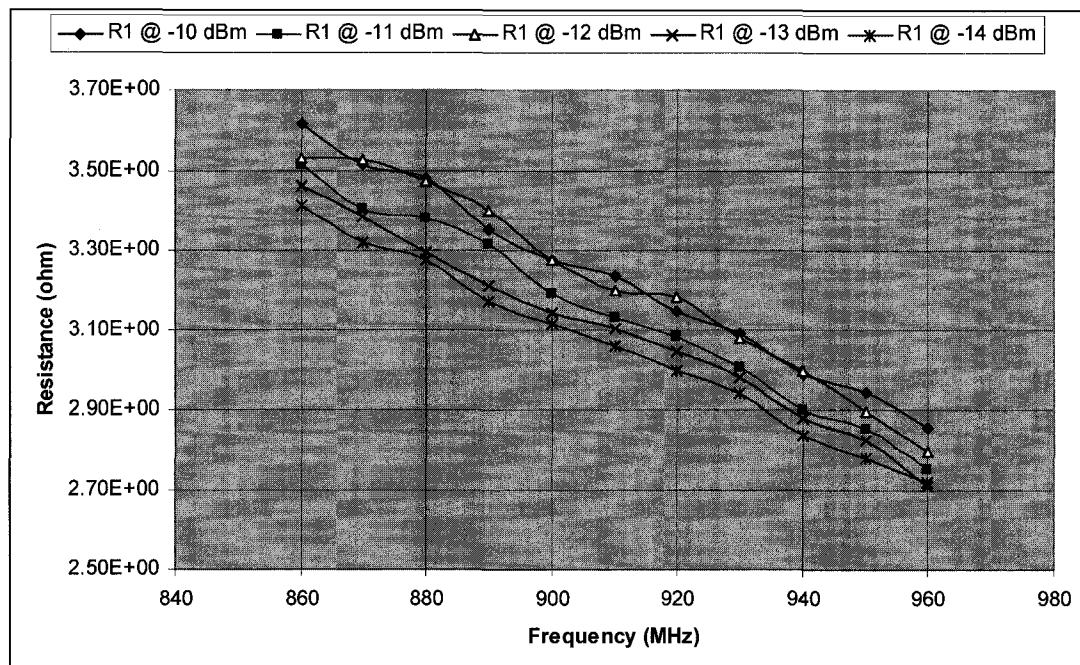


Figure 17 Series resistance measured at five power levels for one ASIC

Figure 17 presents resistance measurement data for one ASIC at five power levels. The

frequency variation of the series resistance indicates a consistent behavior in terms of slope. There are also observed lower values of resistance for lower power level. The maximum difference between the functions of series resistance (vs. frequency) is under 0.25 ohm. This is equivalent with $\Delta R_{\max} \cong 8\%$.

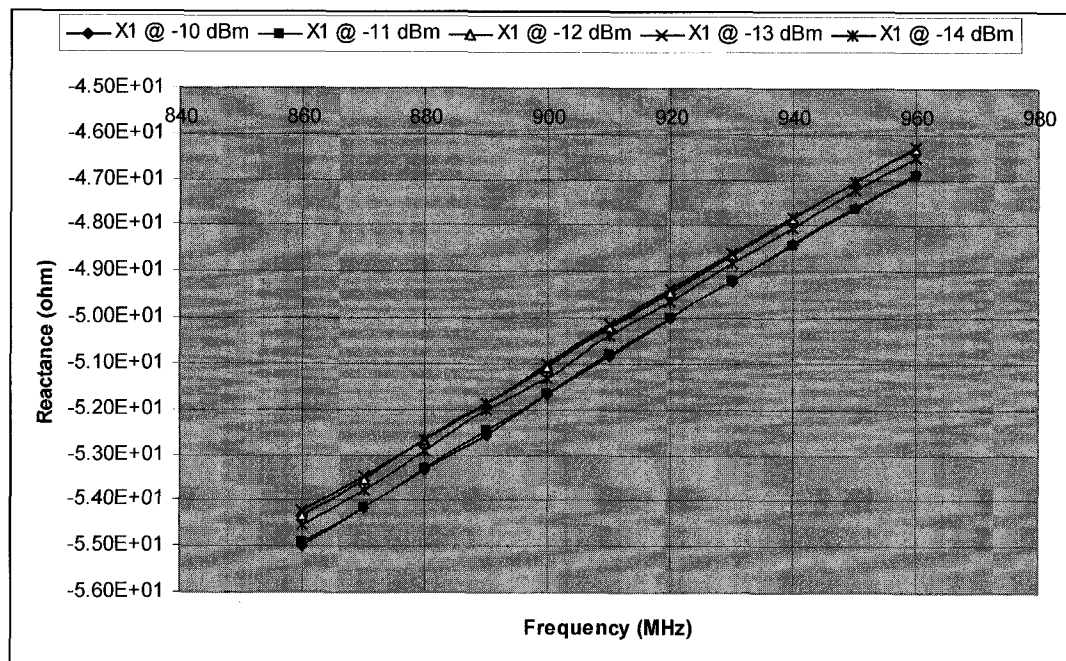


Figure 18 Series reactance measured at five power levels for one ASIC

Figure 18 shows the frequency variation of the series reactance; it has also a consistent behavior in terms of slope. The maximum difference between the functions of series reactance (vs. frequency) is under 1 ohm. This is equivalent with $\Delta X_{\max} \cong 2\%$. These small variations are in agreement with data presented in Table 4 where capacitance values are very close to each other at different power levels.

The comparison of input impedance for different ASICs at the same power levels does indicate the same range of differences. In absence of a large batch of measured data it is assumed that a normal distribution would describe the best the spread of impedances.

3.2.2.3 Sources of Error

For the purpose to have one impedance function representing measurement data, impedance of the four ASICs are averaged at -13 dBm input power level and plotted in the Figure 19. The detailed data is available in Appendix 5.

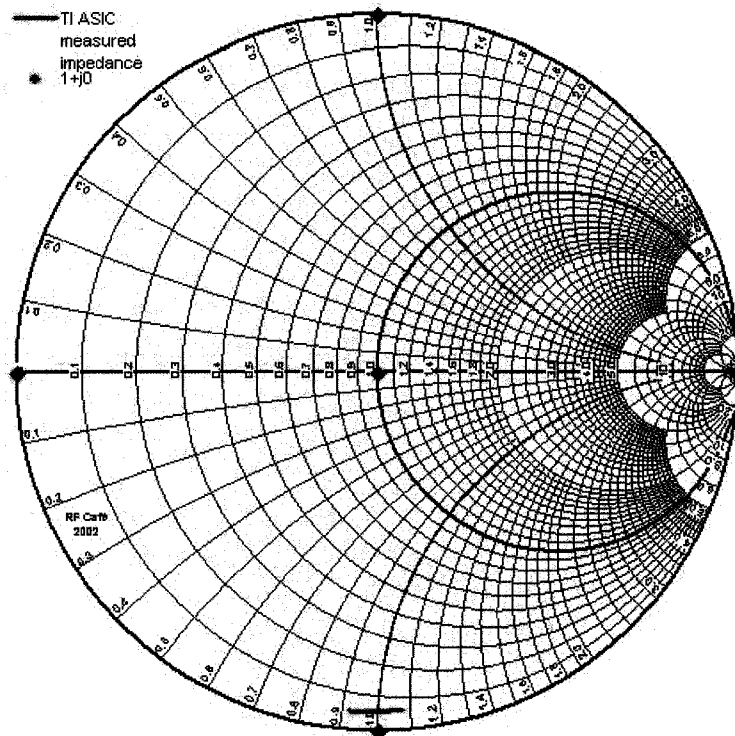


Figure 19 Average of four ASICs impedance at -13 dBm input power level

The comparison between datasheet (Figure 14) and measurement data (Figure 19) indicates a significant difference. The resistance measured is 5.5 to 6 ohm lower than the datasheet values. The reactance measured is 8 to 9 ohm also lower than the datasheet values. In order to explain these differences it is important to analyze the sources of error.

The ASIC it is a small dipole antenna with size $\lambda/40$. The Polyethylene Terephthalate

(PET) substrate attached to the pads and the cardboard box supporting the ASIC during measurement are assumed to be the major contributors to the impedance difference. Future work using simulation with a model including these materials will verify the magnitude of this error.

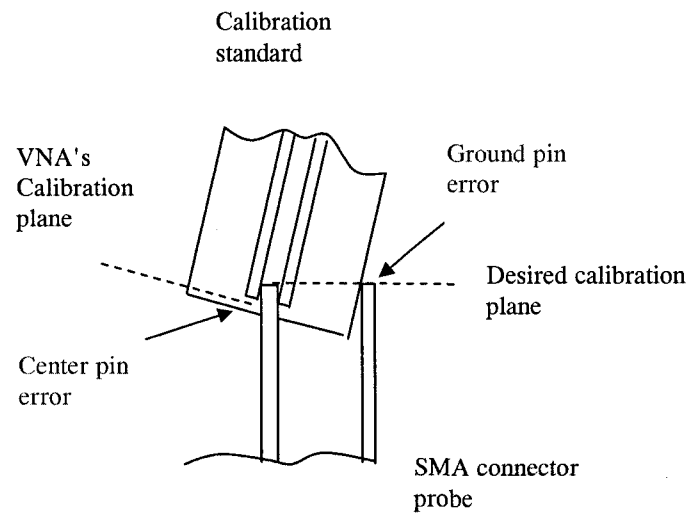


Figure 20 VNA's calibration error sources

Figure 20 shows sources of error introduced during the VNA's calibration. The SMA connector's "calibration plane" is not accurately located at the tip of the pins. When the calibration standards ("Open"; "Short" and "Load") were connected by simply touching the center pin of the SMA probe into the calibration standard center pin, there was a small difference associated with "center pin error". "Ground pin error" was introduced by the location of the SMA's ground pin touching the outside of the calibration standard. These two errors are translated in a phase difference of the RF signal traveling on a shorter path of the transmission line inside the calibration standard.

3.2.3 Determination of the Impedance Matching Point

The matching point of choice is the ASIC's impedance at central frequency of 910 MHz and -13 dBm input power level. The datasheet and the measurement present different values:

1. Datasheet matching point: $Z_D = 10 - j60.8$ ohm
2. Measurement matching point: $Z_M = 3.1 - j50$ ohm

The respective conjugate antenna impedance matching points are:

3. Datasheet matching point: $Z_{AD} = 10 + j60.8$ ohm
4. Measurement matching point: $Z_{AM} = 3.1 + j50$ ohm

We use both of them for building two different prototypes. The performance between the prototypes will indicate the sensitivity of the design relative to the usual matching point, which is given in the datasheet.

3.3 Antenna Modeling

As previously described, the antenna selected for this project is a variation of a bow-tie antenna combined with tapered ends. The design process is using electromagnetic simulation of the antenna, modeled with Ansoft HFSS software package.

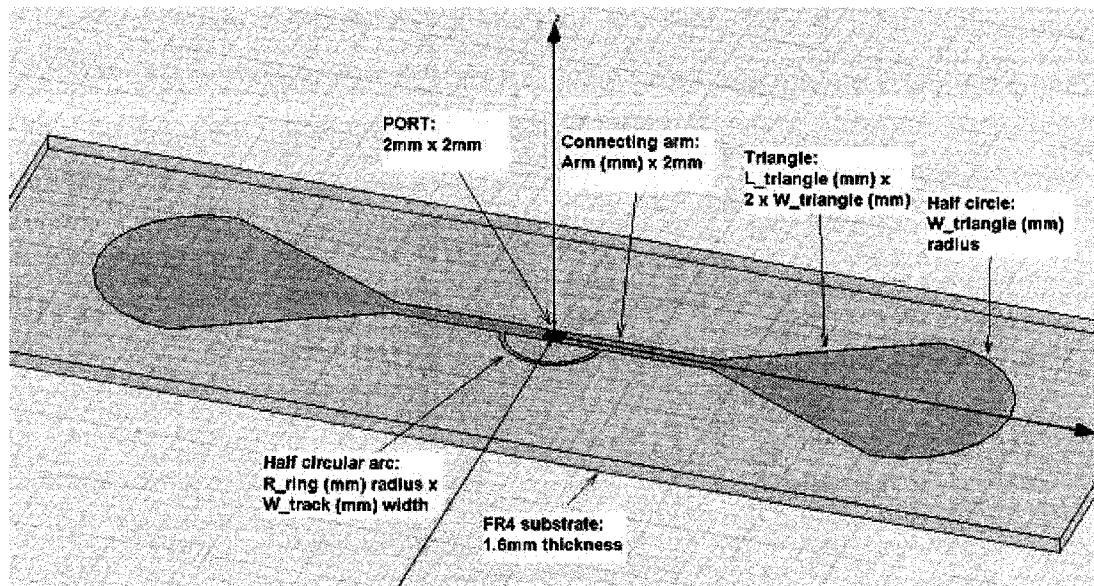


Figure 21 Antenna modeling with Ansoft HFSS software package

Figure 21 introduces various elements of the antenna model and the associated parameters:

- The antenna radiating element uses copper material and has a plane structure centered at origin. Five independent parameters seen in the Figure 21 (Arm; L_{triangle} ; W_{triangle} ; R_{ring} ; W_{track}) are associated with dimensions of simple geometric forms that are united in the antenna radiating element. The names are chosen for easy identification.
- FR4 substrate has two parameters: thickness and relative permittivity. For prototype fabrication the thickness is set to the nominal value of 1.6 mm.
- The "PORT" contains the excitation vector required by the simulation and has fixed dimensions of 2 x 2 mm.

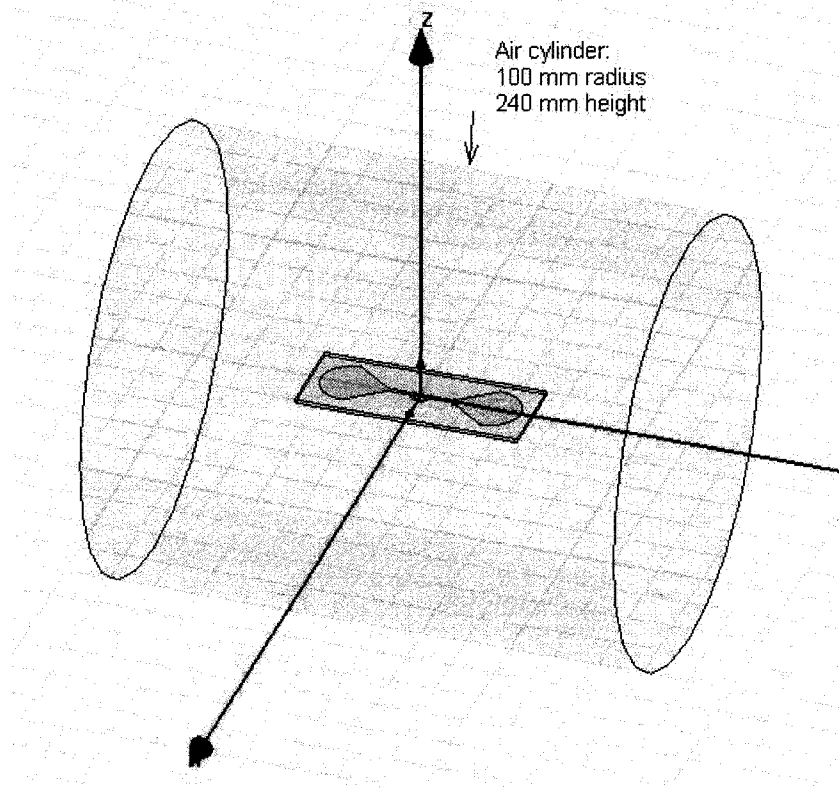


Figure 22 Finite air space used for simulation for antenna modeling

As represented in Figure 22, antenna modeling process requires a finite "air space" assigned for simulation of the electromagnetic field around the antenna. The geometry of this space is a cylinder. The size of the cylinder was experimented from large to small in order to reduce the number of mesh elements used by the FEM. The simulation results were monitored for consistency. The dimensions presented in the Figure 22 for the "air cylinder" were found sufficiently small for a fast completion of the simulation while maintaining consistent results.

3.4 Parametric Study

Parametric study is carried out in respect with the parameters introduced in section 3.3. These antenna parameters are set in incremental steps over a limited range and their influence on antenna impedance is studied using the Smith Chart. Each continuous trace seen in the following figures represent antenna impedance as a function of frequency, simulated between 860 and 960 MHz.

The first goal of the study is to find a pair of independent parameters that adjust the impedance in orthogonal directions, sweeping over the antenna matching point.

The second goal is to increase antenna bandwidth and find the parameters that will reduce the variation of antenna impedance vs. frequency. In other words, the size of the impedance trace on the Smith Chart is preferred small rather than large.

The third goal is to study the sensitivity of the antenna impedance to FR4 permittivity and thickness, in order to be prepared for eventual deviations during prototype fabrication.

3.4.1 Length

There are two parameters changing the antenna length, called “Arm” and “L_triangle”, as seen in Figure 21. Simulations were performed for three different values for each parameter.

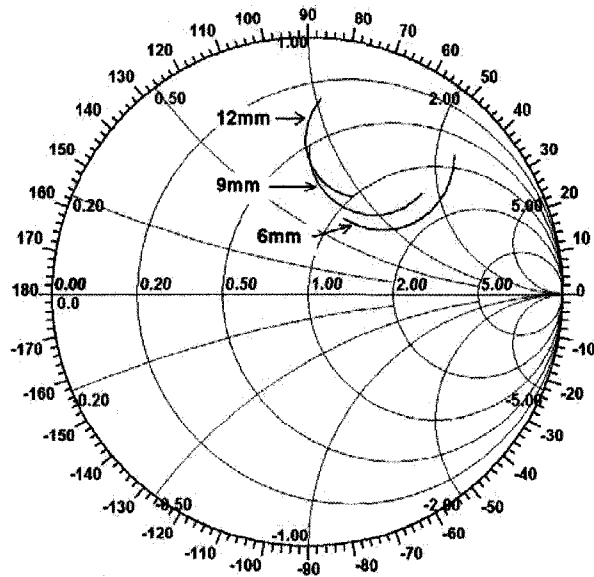


Figure 23 Antenna impedance variation with "Arm" parameter

Figure 23 illustrates antenna impedance variation plotted on the Smith Chart for three consecutive simulations, where "Arm" parameter had the value set to 6, 9 and 12 mm respectively.

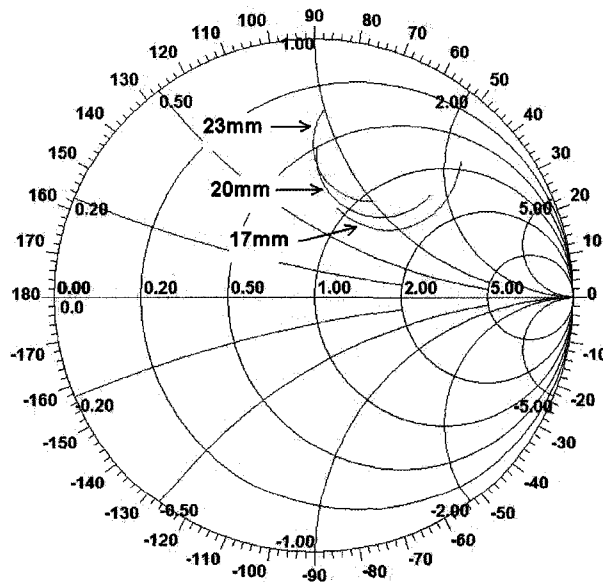


Figure 24 Antenna impedance variation with "L-triangle" parameter

Figure 24 illustrates antenna impedance variation plotted on the Smith Chart for three consecutive simulations, where "L_triangle" parameter had the value set to 17, 20 and 23 mm, respectively.

As seen in Figures 23 and 24, both length parameters have almost identical effects on antenna impedance variation. By making antenna longer or shorter, the impedance is "rotated" clockwise or counterclockwise on the Smith Chart.

3.4.2 Width

The width of the antenna is adjusted with "W_triangle" parameter. Simulations were performed for three different values for this parameter.

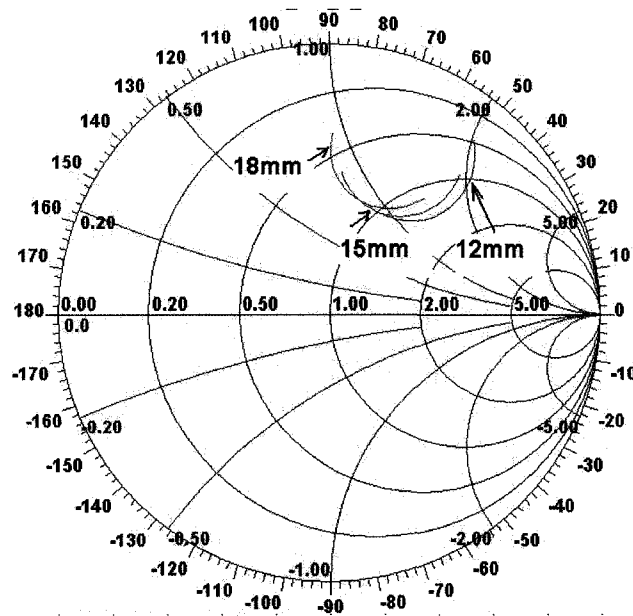


Figure 25 Antenna impedance variation with "W_triangle" parameter

Figure 25 illustrates antenna impedance variation plotted on the Smith Chart for three consecutive simulations, where "W_triangle" parameter had the value set to 7, 10 and 13 mm respectively.

The antenna impedance variation due to change of “W-triangle” parameter has the same behavior as the variation due to change in length presented in the section 3.4.1. It can be noticed that “W-triangle” parameter was changed in 3 mm steps as well as the length parameters in the section 3.4.1. By making antenna wider or narrower, the impedance is “rotated” clockwise or counterclockwise on the Smith Chart.

3.4.3 Radius of the Loop

The antenna element named “Half circular arc” and introduced in Figure 21 is increasing the inductive characteristic for overall antenna impedance. This effect is desired for matching the impedance to any of the two points established in section 3.2.3.

There are practical benefits associated with the use of this antenna element:

- The DC short circuit resistance helps to eliminate the possibility of electrostatic discharge (ESD) from damaging the die input circuitry.
- The closed-loop inductance may couple with the magnetic field present in the near field of reader’s antenna, providing reliable operations for the transponder in this zone.

The “R-ring” parameter adjusts the radius of the “Half circular arc” antenna element. Simulations were performed for three different values for this parameter.

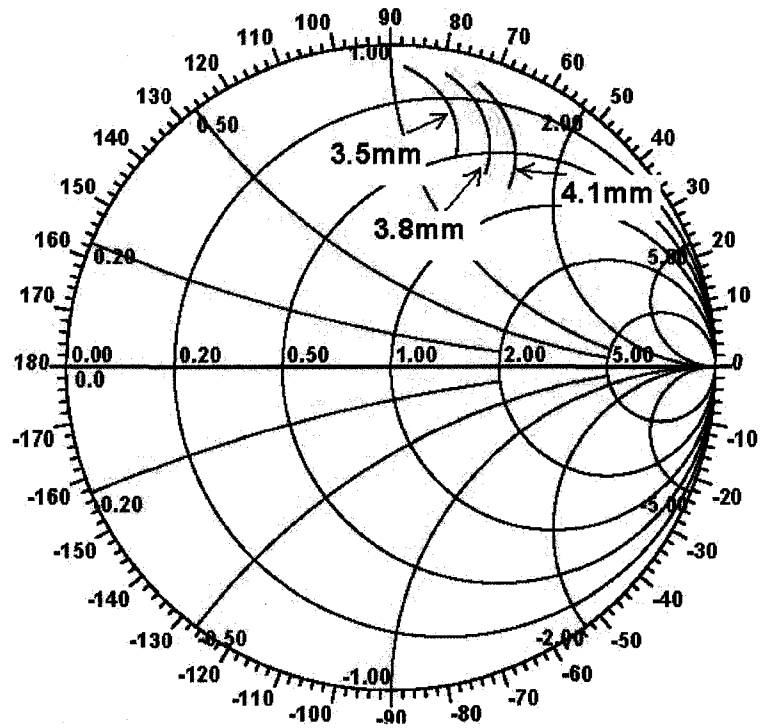


Figure 26 Antenna impedance variation with “R_{ring}” parameter

Figure 26 illustrates antenna impedance variation plotted on the Smith Chart for three consecutive simulations, where “R_{ring}” parameter had the value set to 3.5, 3.8 and 4.1 mm, respectively. As the “R_{ring}” parameter was increased, the antenna impedance on the Smith Chart was translated towards the right of the figure. It is observed a high sensitivity of antenna impedance relative to a small change of this parameter.

3.4.4 Width of the Loop Track

The “W_{track}” parameter adjusts the track width of the “Half circular arc” antenna element presented in the Figure 21. Simulations were performed using two different values for this parameter.

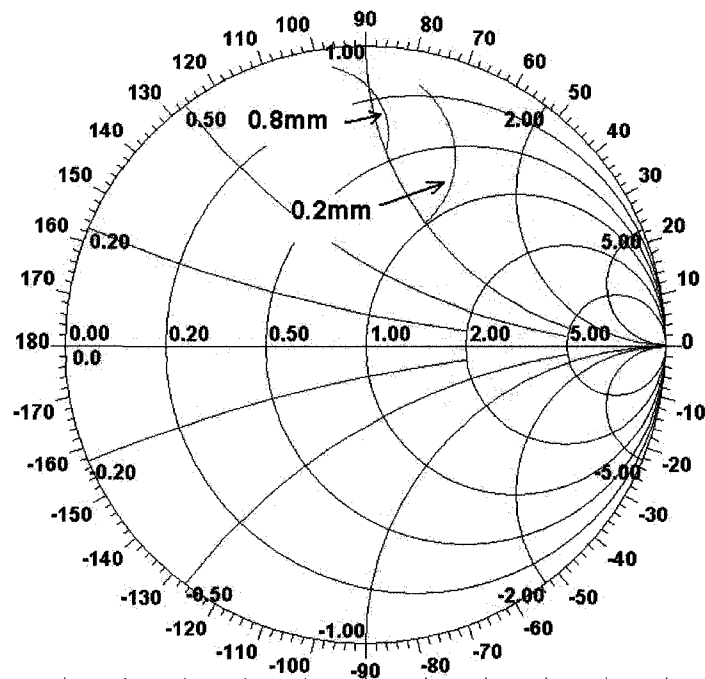


Figure 27 Antenna impedance variation with “W_track” parameter

Figure 27 illustrates antenna impedance variation plotted on the Smith Chart for two consecutive simulations, where "W_track" parameter had the value set to 0.2 and 0.8 mm, respectively. As the "W_track" parameter was increased from 0.2 to 0.8 mm, the antenna impedance on the Smith Chart translated towards the left of the figure. It is observed a high sensitivity of antenna impedance relative to a small change of this parameter.

3.4.5 Thickness and Permittivity of Substrate

These parameters adjust the FR4 substrate properties introduced in the Figure 21. Simulations were performed using two different values for each parameter.

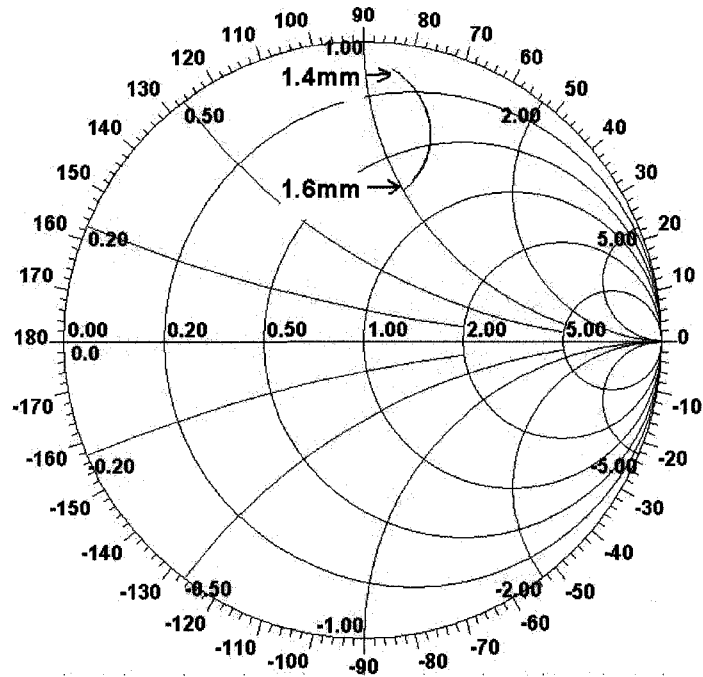


Figure 28 Antenna impedance variation with FR4 substrate thickness

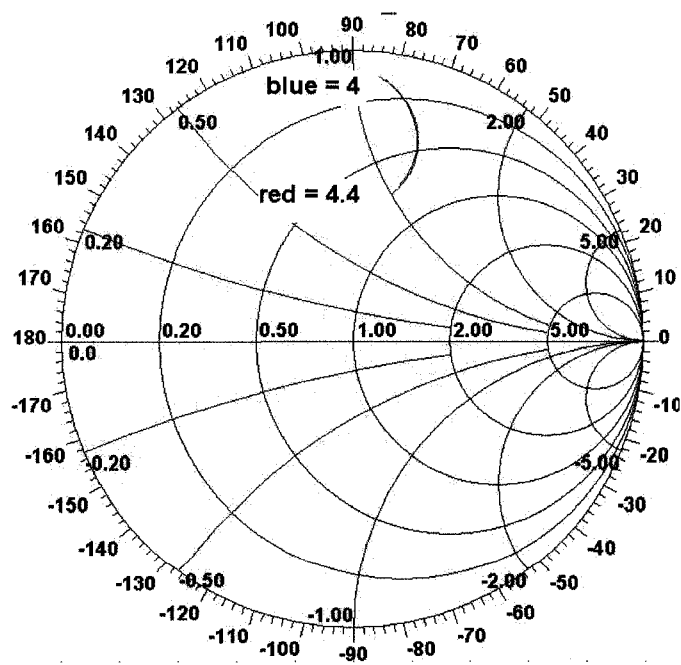


Figure 29 Antenna impedance variation with FR4 substrate relative permittivity

As seen in both Figures 28 and 29, the increase in thickness or relative permittivity generates a similar variation of the antenna impedance. This effect can be described as a “rotation” clockwise on the Smith Chart.

3.4.6 Final Parameters Chosen for Prototypes

The analysis is summarized as follows:

- The “Arm” and “R_ring” are parameters that adjust the impedance variation in nearly orthogonal directions, sweeping over the desired antenna matching point. These directions are illustrated in Figure 30.

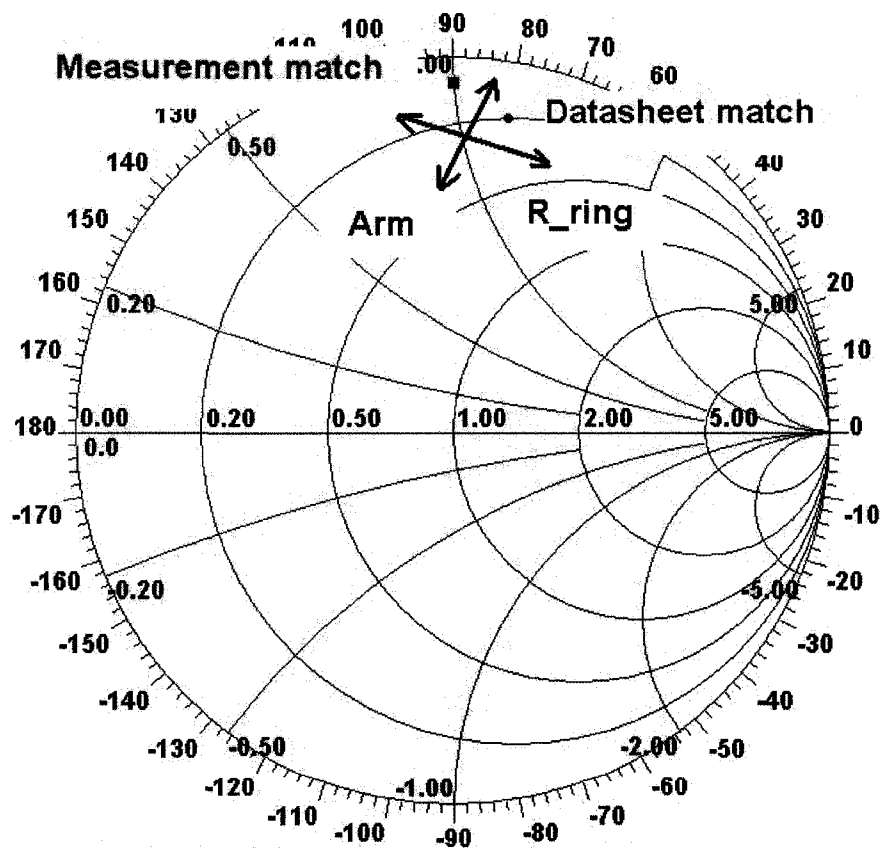


Figure 30 Parameters that change impedance in nearly orthogonal directions

- The “W_triangle” parameter has to be adjusted in connection with “Arm”. In the same way, “W_track” parameter must be adjusted in connection with “R_ring”.
- There are two different antenna lengths between $\lambda/4$ and $\lambda/2$ that offer possible candidates for good impedance matching. Four prototype options are presented in Table 7.

Table 7 Four prototyping options

PROTOTYPE OPTIONS	“Long” Antenna	“Short” Antenna
Datasheet Match $Z_{AD} = 10 + j60.8$	“Long-D” (Figure 32)	“Short-D” (Figure 31)
Measurement Match $Z_{AM} = 3.1 + j50$	“Long-M” (Figure 32)	“Short-M” (Figure 31)

Table 7 indicates the figures showing four options for antenna impedance variation matched to two required matching points determined in section 3.2.3. The differences between the antennas are presented in Table 8.

Table 8 Parameter values for four prototype antennas

PARAMETERS (mm)	“Long-D”	“Long-M”	“Short-D”	“Short-M”
Arm	16	16	14	14
L_triangle	30	30	16.3	16.3
W_triangle	15	15	12.7	12.7
R_ring	5.3	4.7	3.8	3.45
W_track	1	1	1	1
Overall antenna length	126	126	90	90

Table 8 presents the parameter values for all four prototype antennas. These values were obtained as result of multiple simulations, which sequence is not detailed in this report.

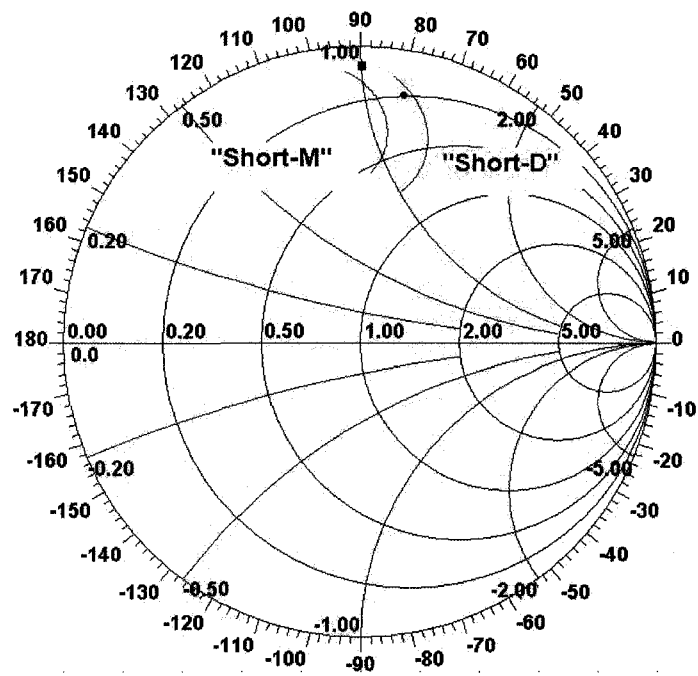


Figure 31 Two "Short" antennas impedance variation

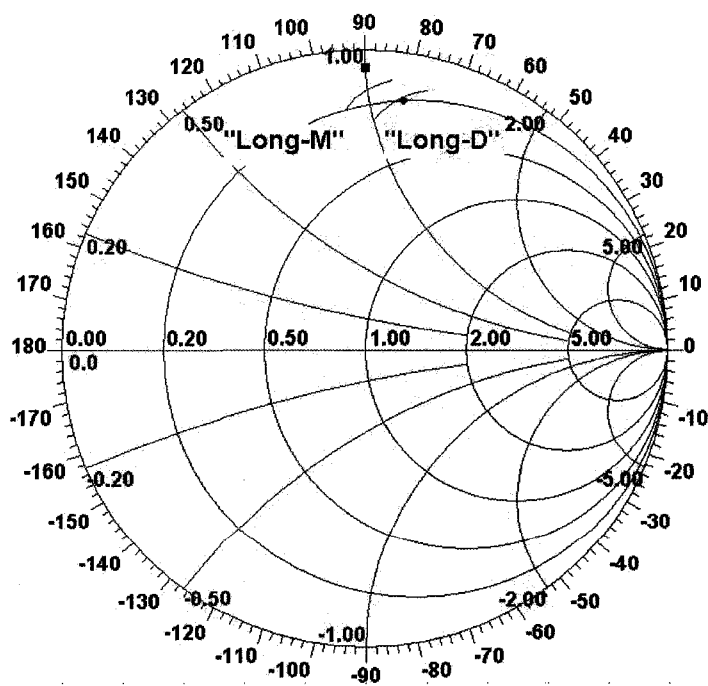


Figure 32 Two "Long" antennas impedance variation

Figures 31 and 32 present all four prototype antennas impedance variations matched to the indicated impedance points.

3.5 Measurement of Antenna Prototypes

The prototype antennas, with parameters presented in Table 8, were fabricated using FR4 substrate of 1.6 mm thickness plated with copper. One "Long" and one "Short" prototype are plotted in Figures 33 and 34 at approximate 1:1 scale.

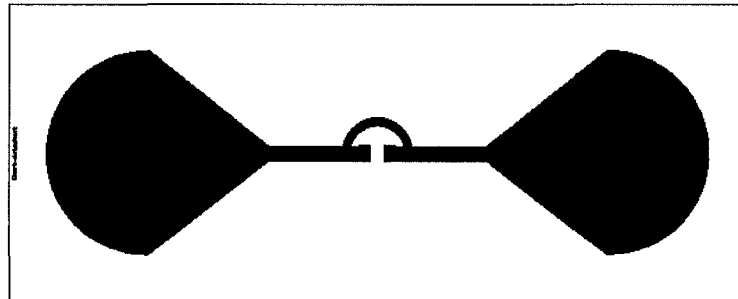


Figure 33 "Short" transponder antenna – copper layout

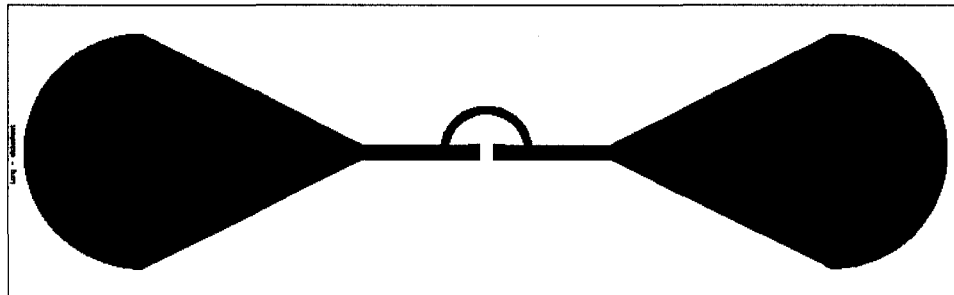


Figure 34 "Long" transponder antenna – copper layout

Measurements of the four antennas are performed. Impedance measurements are presented first - swept between 860 and 960 MHz - then gain and radiation pattern.

3.5.1 Measurement of Antenna Impedance

Antenna impedance measurement was performed using the same Vector Network Analyzer (VNA) AGILENT 8722ES. The setup and calibration of the VNA was identical with the procedure described in section 3.2.2.1 for measurement of ASIC impedance.

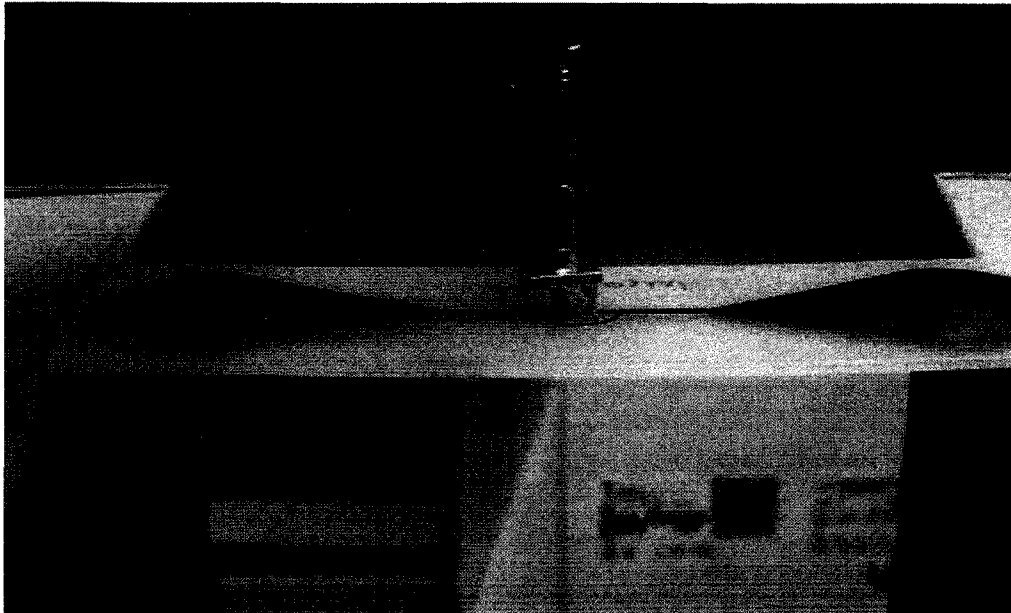


Figure 35 **Antenna impedance measurement setup**

Figure 35 shows the setup for antenna measurement. This setup is intended to minimize the interference from objects present in the immediate vicinity.

3.5.1.1 Measurement Results

All four antenna prototypes were measured and the impedance plots on the Smith Chart are shown in Figures 36 to 39. Numerical data is presented in Appendix 6 and was further used for mismatch loss calculations and range estimate.

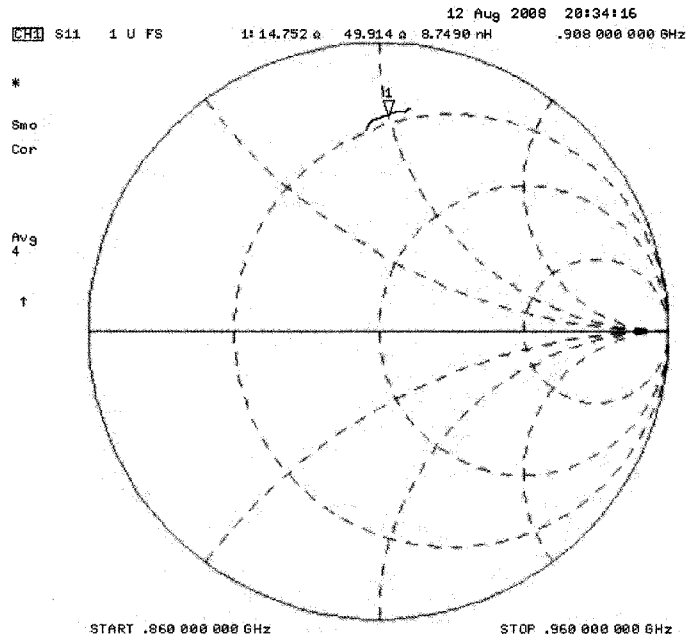


Figure 36 Impedance of "Long-D" antenna prototype

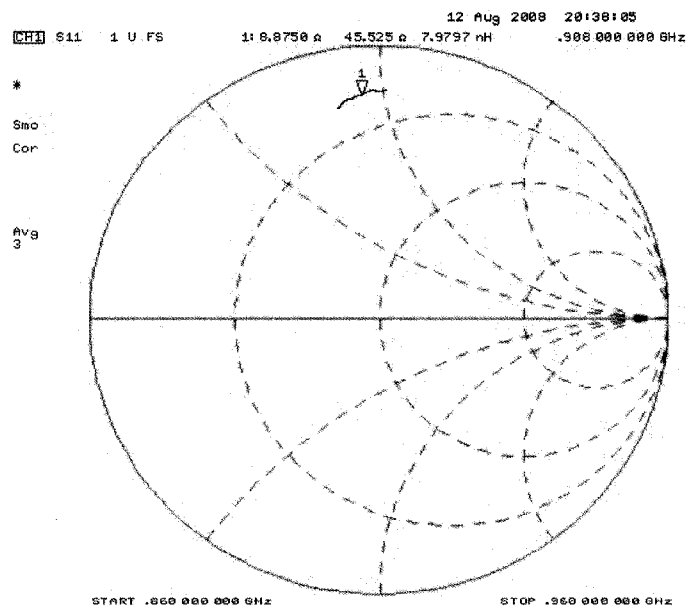


Figure 37 Impedance of "Long-M" antenna prototype

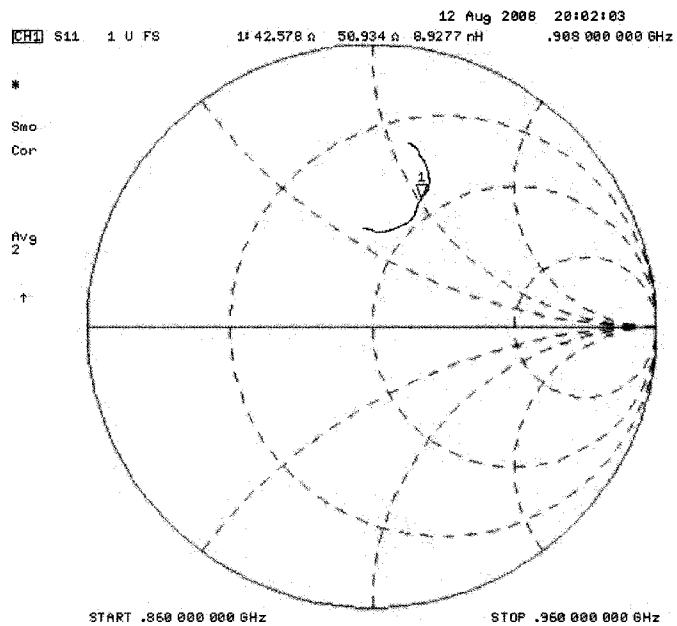


Figure 38 Impedance of “Short-D” antenna prototype

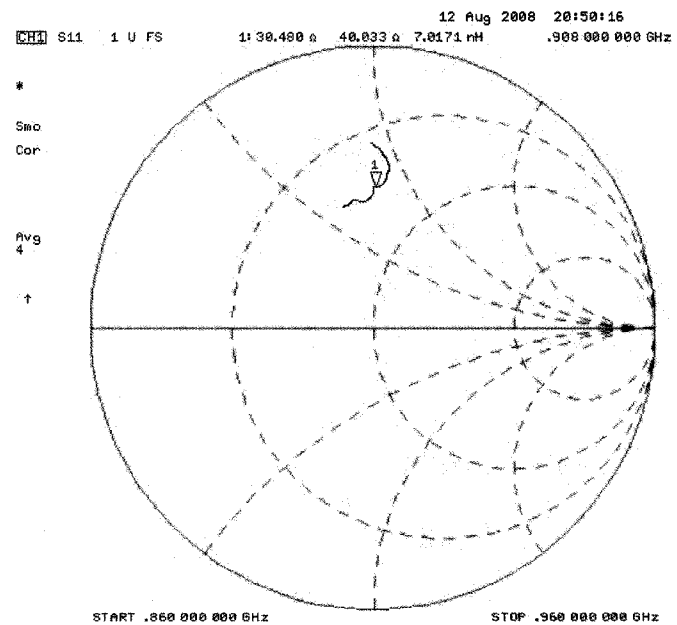


Figure 39 Impedance of “Short-M” antenna prototype

The reflection coefficient due to impedance mismatch is calculated relative to 50 ohm transmission line. In this case, the formulas presented in sections 2.1.2 and 2.1.3 apply.

The raw data measurement and detailed calculations are presented in Appendix 8.

Table 9 Power transmission coefficient for “Short-M” antenna prototype

	860 MHz	910 MHz	960 MHz
Reflection Coefficient $ \Gamma $ relative to 50 ohm (linear)	0.656	0.5	0.4427
Power Transmission Coefficient = $1 - \Gamma ^2$ (dB)	-2.44356	-1.25475	-0.94731

Table 9 presents the summary results for the calculation of the power transmission coefficient based on measured reflection coefficient of the "Short-M" antenna prototype (see impedance plot in Figure 39). These results are used for determination of the maximum antenna gain on a following section of this report.

3.5.1.2 Sources of Error

The visual inspection of all four measured impedances shows an overall 10 degrees offset compared with the designed impedance values seen in Figures 31 and 32. Also, all four results show an overall offset towards the center of the Smith Chart. This offset is more visible for the “Short” antenna prototypes. This indicates a larger resistance of the measured antennas. The relative position of the impedances on the Smith Chart between the “Short” prototypes is in agreement with the design impedance plotted in Figure 31. Similar observation can be made about the relative impedance between the “Long” prototypes, found in agreement with Figure 32.

The analysis of error sources includes all considerations presented in section 3.2.2.3. These refer to objects in vicinity and calibration issues around the SMA connector probe. The most influential object is the VNA’s cable, which is placed inside the antenna’s reactive and radiating near-fields. This cable changes antenna’s radiation pattern.

3.5.2 Measurement of Maximum Gain

The gain transfer method, as described in section 2.3, was employed to determine maximum gain. All measurements were done inside the anechoic chamber in Microwave and Wireless Research Laboratory at Dalhousie, in order to minimize the multipath interferences. The instrument used for these measurements was the Vector Network Analyzer (VNA) AGILENT 8722ES.

3.5.2.1 Instrument Calibration and Measurement of Offset

This preliminary stage has the purpose to determine the offset introduced by cables insertion loss (IL) and small impedance mismatches in the connectors.

Initially, the instrument was calibrated for transmission measurement (one-port plus through) with chamber cables disconnected. The calibrated return loss at the generator port is 37 dB. The return loss at the load port is 18 dB, which is dominated by the flexible cable attached to the test port (18 dB return loss). The return loss is defined as: $RL = -20 \cdot \log(|\Gamma|)$, where $|\Gamma|$ is the magnitude of the reflection coefficient.

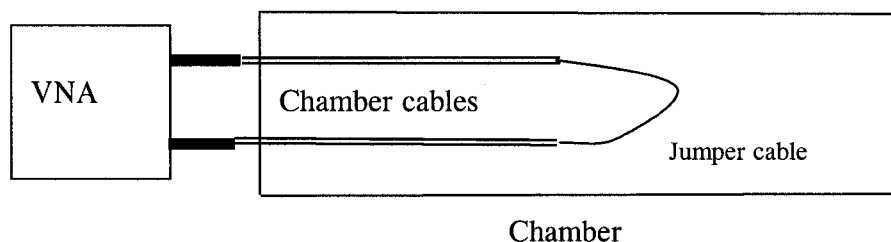
The transmission uncertainty of the VNA calibration is calculated using only the term $(1 \mp |\Gamma_G| \cdot |\Gamma_L|)^2$, presented in section 2.3. The uncertainty interval expressed in dB's has the following formula: $U_\tau = -20 \cdot \log(1 \mp |\Gamma_G| \cdot |\Gamma_L|)$. The result is calculated as -0.015 to +0.015 dB interval.

A 15 ft coaxial cable was used as a jumper between the ends of the cables going inside the anechoic chamber. The ends of these cables could not be connected directly, being attached to the chamber fixtures.

Table 10 Jumper cable insertion loss

	860 MHz	910 MHz	960 MHz
Insertion Loss (dB)	11.22	11.63	11.94

Table 10 presents the measurement results of the insertion loss of the jumper cable, connected directly between the calibrated ports of the VNA. The measurement uncertainty is calculated with the formula for M presented in section 2.3, where this time $|\Gamma_R| = |\Gamma_T| = 0.2$ are the magnitudes of reflection coefficients calculated using the input and output return loss of the jumper cable of 14 dB. The measurement uncertainty is found between -0.256 to +0.261 dB.

**Figure 40** Offset measurement setup

In the following step, as shown in Figure 40, the chamber cables were connected to the instrument and the jumper installed inside the chamber, between the opposite ends.

Table 11 Chamber cables insertion loss

	860 MHz	910 MHz	960 MHz
Total Insertion Loss (dB)	17.06	17.63	18.01
Chamber cables Insertion Loss (dB) = Total - Jumper	5.84	6	6.07

Table 11 presents the chamber cables insertion loss calculated as a difference between the

total insertion loss measured with the setup from Figure 40 and the jumper cable insertion loss presented in Table 10.

3.5.2.2 Calculation of the Reference Transmission Level

The reference transmission level was determined by measuring a standard antenna. The reference standard antenna used was a double ridge pyramidal horn, model SAS-200/571, manufactured by A.H. Systems Inc. The calibrated gain at 3 m and 900 MHz is 7.2 dBi. In absence of detailed information, this value is assumed constant over the 860 to 960 MHz band. The Voltage Standing Wave Ratio (VSWR) = 2:1. The magnitude of the reflection coefficient can be computed using the well known formula [5]:

$$|\Gamma| = (\text{VSWR}-1) / (\text{VSWR}+1) = 0.333$$

The probe existent inside the chamber is a broadband linearly polarized log periodic antenna, model 201031, manufactured by Tecom Industries Inc. The datasheet gain at 900 MHz is 7.5 dBi. In absence of detailed information, this value is also assumed constant over the 860 to 960 MHz band. VSWR=2:1 ($|\Gamma| = 0.333$). The cross polarization is 20 dB.

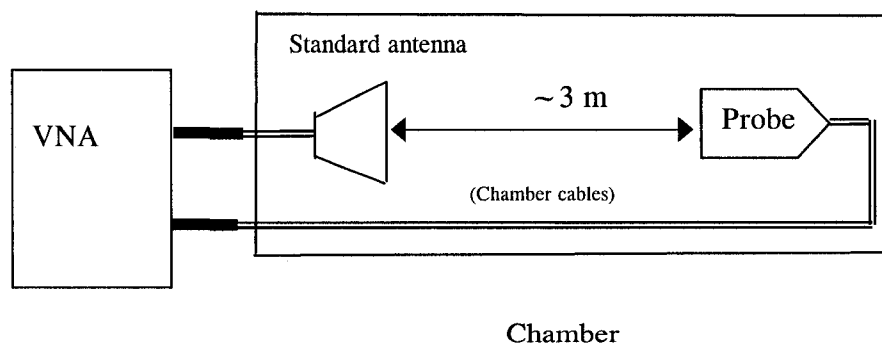


Figure 41 Transmission calibration setup using a standard antenna

Figure 41 presents the setup for measuring the transmission level of the standard antenna.

The approximate 3 m range inside the chamber sets the measurement in far-field. Two measurements were performed: first with the horn transmitting and the second with the probe transmitting. The raw data is presented in Appendix 7.

Table 12 Summary of standard antenna transmission measurement

	860 MHz	910 MHz	960 MHz
Free Space Loss @ 3m (dB)	-40.68	-41.17	-41.63
Chamber cables IL (dB)	-5.84	-6	-6.07
Probe gain (dB)	7.5	7.5	7.5
Standard antenna gain (dB)	7.2	7.2	7.2
Calculated Transmission Loss	-31.82	-32.47	-33
<i>Measured Transmission Loss (dB)</i>	<i>-32.1</i>	<i>-32.54</i>	<i>-33.42</i>
Error (dB) = Calculated - Measured	-0.72	0.07	0.42

Table 12 gives the summary of the standard antenna transmission measurement. The "Free Space Loss @ 3m" was computed with the formula presented in section 2.1.8. The "Chamber cables IL" data was imported from Table 11. The "Calculated Transmission Loss" was computed using FRIIS formula in logarithmic format. The "Measured Transmission Loss" was collected from the VNA using the setup presented in Figure 41.

For verification purposes, the "Error" is calculated in the last line of the table as difference between "Calculated Transmission Loss" and "Measured Transmission Loss". The measurement uncertainty due to mismatch is within -0.41 to +0.43 dB. This is added to the horn calibration accuracy ± 1 dB for a total uncertainty interval of -1.41 to 1.43 dB. As result, the error calculated is within acceptable limits and the transmission calibration for gain measurement is assessed as adequate.

Table 13 **Reference Transmission Level**

	860 MHz	910 MHz	960 MHz
Reference Transmission Level = RTL (dB)	-39.02	-39.67	-40.2

Table 13 presents the reference transmission level, which is obtained by subtracting the standard antenna gain from the calculated transmission loss from Table 12.

3.5.2.3 Measurement Results

In the last stage of gain transfer method, one “Short-M” and one “Long-M” prototype antennas replaced the standard antenna in the setup presented in the Figure 41.

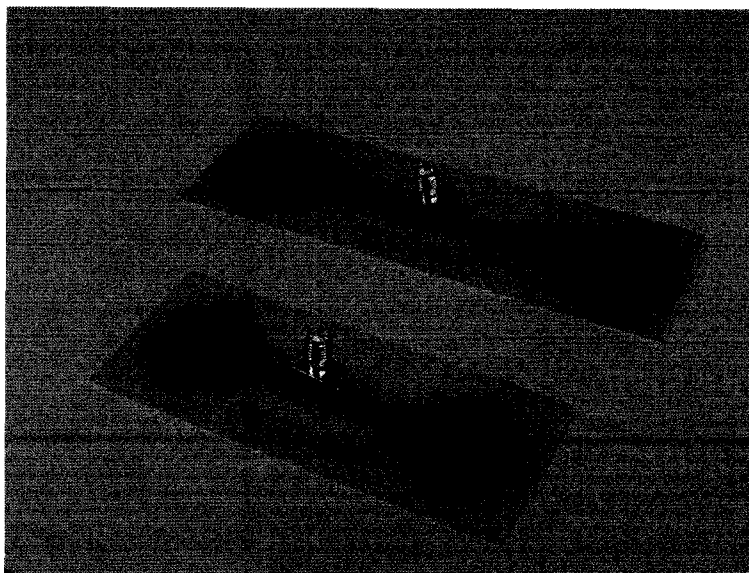


Figure 42 **Prototype antennas prepared for maximum gain measurement**

Figure 42 shows prototype antennas with SMA connectors attached, in preparation for maximum gain measurement.

Detailed calculations are presented only for the “Short-M” antenna prototype. Only final results are presented for the “Long-M” antenna prototype. The transmission data was collected in two configurations: first measurement had the prototype antenna transmitting and the second had the probe transmitting. The raw data is presented in Appendix 9. Their average is presented as "Measured Transmission Loss with Antenna Prototype" in Table 14.

Table 14 Maximum gain calculation for “Short-M” antenna prototype

	860 MHz	910 MHz	960 MHz
Measured Transmission Loss with Antenna Prototype = MSL (dB)	-40.2	-39.17	-39.1
Reference Transmission Level = RTL (dB) (from Table 13)	-39.02	-39.67	-40.2
Calculated maximum gain with mismatch loss = MSL - RTL (dBi)	-1.18	0.5	1.1
Maximum Gain = maximum gain with mismatch - power transmission coefficient (dBi) (from Table 9)	1.26	1.75	2.05

Table 14 presents the summary of maximum gain calculation for the “Short-M” antenna prototype. The maximum antenna gain including the mismatch losses is computed by subtracting the reference transmission level (determined by using the standard antenna) from the VNA measurement data (the first row in Table 14). The maximum gain is then determined by subtracting also the mismatch losses (presented in Table 9).

The measurement uncertainty due to mismatch is calculated between -0.45 and +0.47 dB. This is added to the horn calibration accuracy of ± 1 dB for a total uncertainty interval of -1.45 to 1.47 dB. The expected range for this size dipole is 1.5 to 1.9 dBi with no significant variation over 860 to 960 MHz frequency band. “Short-M” antenna prototype

maximum gain is calculated as the average of the values in Table 14, producing a value of 1.68 dBi. In a similar way, maximum gain calculated for the “Long-M” antenna prototype is 1.82 dBi. The “Short-D” and “Long-D” antennas have identical size with “Short-M” and “Long-M”, respectively, and their gains is assumed to have same values.

3.5.2.3 Sources of Error

The errors for maximum gain measurement are compounded from multiple sources, such as:

- Error of impedance measurement and calculated antenna reflection coefficient
- Absence of impedance and gain variations with frequency for the pyramidal horn used as standard antenna for transmission calibration. These antenna parameters were assumed constant.
- Absence of impedance and gain variations with frequency for the probe antenna used in the anechoic chamber. These antenna parameters were assumed constant.

Another method for determination of maximum gain is the measurement of the radiation pattern as described in the section below.

3.5.3 Radiation pattern measurement

These measurements were done using the automated system with the anechoic chamber in the Microwave and Wireless Research Laboratory at Dalhousie University. The distance of 3 m between antenna prototype and probe makes the operations in the “Far-field” region.

The data was collected in steps of 6 degrees each for both φ and θ axis, for both vertical and horizontal polarizations.

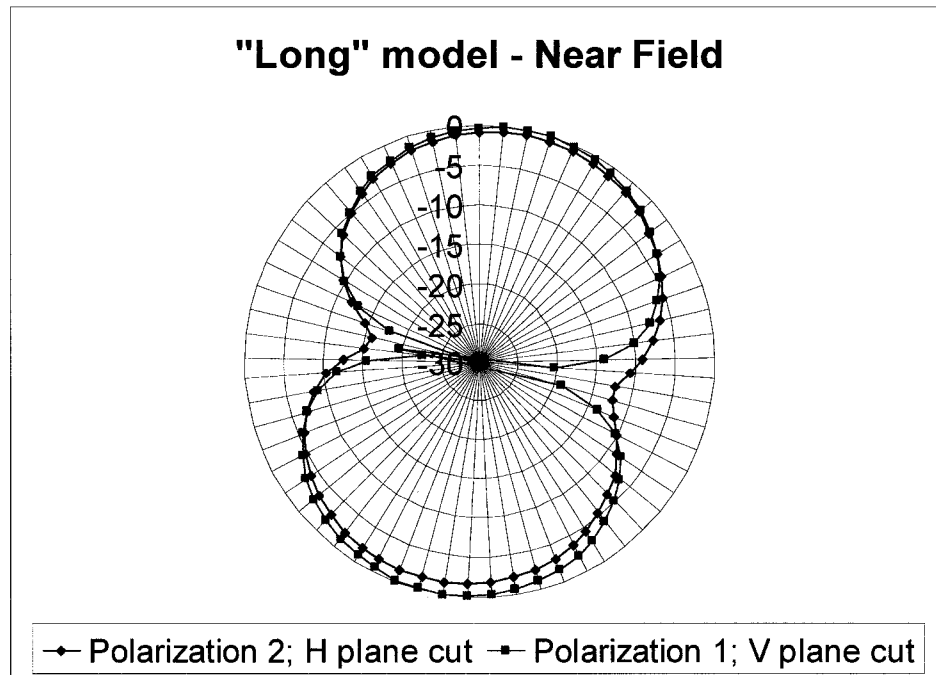


Figure 43 Measured Near-field radiation pattern for "Long-M" antenna prototype

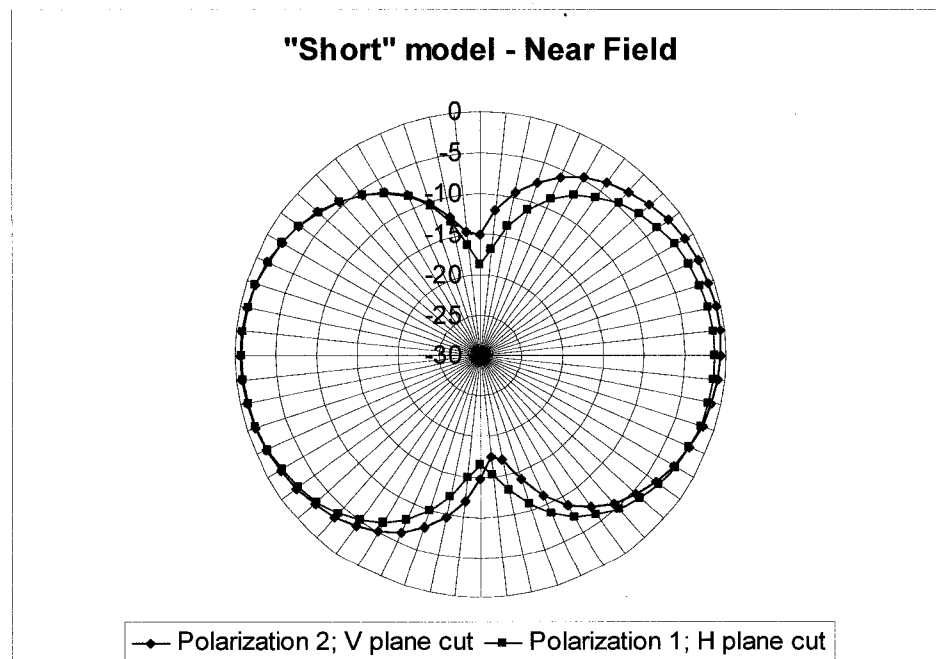


Figure 44 Measured Near-field radiation pattern for "Short-M" antenna prototype

Figures 43 and 44 present the measured radiation pattern for "Short-M" and "Long-M" prototype antennas. Each figure has two series plotted. Each series represents measurement in a different polarization, either vertical or horizontal. The presentation in a two-dimensional plot offers an easy comparison relative to each other. There is a noticeable offset of both patterns from the horizontal and/or vertical axis due to inaccurate placement of the antenna at the beginning of the measurement.

This pattern was expected and is in agreement with the theoretically estimated pattern presented in Figure 7. By integration over the radiation pattern, maximum gain was computed to 2.1 dBi for both models. This value is outside the expected range of 1.5 to 1.9 dBi. Unfortunately, the conversion software did not produced reliable results and the cause of the error remains to be researched.

3.6 Prototype Transponders Range

3.6.1 Range Estimation

Range estimation is only calculated with maximum gain using the Friis transmission equation presented in section 2.1.8. In it, the transmitter (t) is the RFID reader and the receiver (r) is the transponder.

The following parameters are set:

- Transmitter power is set to be +26 dBm=398.1 mW
- ASIC received power is set to be -10 dBm=0.1 mW. As presented in section 3.2, the ASIC input power threshold is -13 dBm. Knowing that the reader uses ASK modulation, 3 dB in difference accounts for half power loss during reader's communications.
- $PolarizationLossFactor = \cos^2 \psi = 1$

The reader's antenna is designed for RFID applications and is manufactured by Symbol Technologies. The model is AN400-CB66203WR, has dual inputs, circular polarization and VSWR of 2:1. The maximum gain was measured inside anechoic chamber using the same setup and method presented for antenna prototypes.

Table 15 Maximum gain calculation for reader's antenna

	860 MHz	910 MHz	960 MHz
Measured Transmission Loss = MSL (dB)	-30.4	-32.2	-34
Reference Transmission Level = RBL (dB)	-39.02	-39.67	-40.2
Calculated maximum gain $G_{or} = MSL - RBL$ (dBi)	8.62	7.47	6.2

Table 15 presents the maximum gain measurement of the RFID reader's antenna. The

measurement uncertainty due to mismatch is calculated inside the interval -0.41 to +0.43 dB. The standard antenna calibration accuracy is ± 1 dB. The measurement uncertainty due to the cross polarization (20 dB) of the probe (which is linearly polarized antenna) while measuring a circularly polarized antenna is between -0.915 dB and 0.828 dB [13]. Therefore, the total range of uncertainty is -2.32 to +2.25 dB. As result, the maximum gain has acceptable calculated values.

For further use, the gain of the Symbol antenna is adopted as constant value over the 860 to 960 MHz frequency band of 7 dBi (5 linear). If better accuracy is required, measured antenna impedances should provide better mismatch loss that can be computed over this frequency band.

The range formula is then:

$$R = \frac{\lambda}{4\pi} \sqrt{G_{0r} \cdot G_{0r} \cdot (1 - |\Gamma_r|^2) \cdot \frac{398.1}{0.1}} \quad \text{where } \lambda = \frac{c}{f} = \frac{300}{f_{MHz}} \quad (\text{m}) \text{ is the wavelength,}$$

$G_{0r} = 5$ is the reader's antenna maximum gain, $G_{0r} = 1.4723$ is the transponder's antenna maximum linear gain for the "Short" model (or $G_{0r} = 1.52$ for the "Long" model)

The transponder's power transmission coefficient $1 - |\Gamma_r|^2$ is calculated using the antenna impedance measured in the section 3.4.1.1 relative to the ASIC's datasheet conjugate impedance presented in the section 3.2.2.

The transponder is represented by a generator (in this case the antenna) connected to a load (in this case the ASIC) and both impedances are complex numbers. The *power wave reflection coefficient* is defined by Kurokawa [8] as:

$$s = \frac{Z_L - Z_A^*}{Z_L + Z_A}$$

where Z_L is the load impedance and Z_A is the antenna impedance. Therefore, the power transmission coefficient can be written as $1 - |\Gamma_r|^2 = 1 - |s|^2$ [6] [7].

Table 16 Power transmission coefficient for the "Short-M" transponder

ASIC impedance		Antenna impedance		Reflection Coefficient (Γ)	Power Transmission coefficient
R_L (Ω)	X_L (Ω)	R_s (Ω)	X_s (Ω)		
9.10E+00	-6.26E+01	1.97E+01	4.53E+01	0.535466991477019-0.279302861143432j	0.635265013
8.90E+00	-6.19E+01	2.09E+01	4.62E+01	0.533043597885855-0.246131690418692j	0.655283714
8.70E+00	-6.12E+01	2.35E+01	4.71E+01	0.546825680218402-0.198622130683588j	0.661530925
9.79E+00	-6.02E+01	2.77E+01	4.70E+01	0.535844858010814-0.163568519379353j	0.686115628
9.58E+00	-5.95E+01	3.08E+01	4.30E+01	0.594205698797543-0.166063110658325j	0.619342631
9.37E+00	-5.89E+01	3.02E+01	4.04E+01	0.611634570565813-0.182212594629706j	0.592701722
9.17E+00	-5.83E+01	3.17E+01	3.81E+01	0.639282967309744-0.178450342918213j	0.559472763
8.98E+00	-5.77E+01	3.03E+01	3.48E+01	0.658680730335372-0.199064672464585j	0.526512952
9.15E+00	-5.50E+01	2.92E+01	3.40E+01	0.633181130217124-0.201411425413068j	0.558515094
8.96E+00	-5.45E+01	2.92E+01	3.27E+01	0.645490711554277-0.201599460703063j	0.542699399
8.78E+00	-5.39E+01	2.88E+01	3.08E+01	0.66053735745249-0.208815557859995j	0.520086462

Table 17 presents the calculation of the power transmission coefficient for the "Short-M" transponder calculated relative to the datasheet point, using an Excel spreadsheet.

Table 17 Range estimation for the "Short-M" transponder

F (MHz)	Power Transmission coefficient	RANGE Estimate (m)
860	0.635265	3.768679
870	0.655284	3.783603
880	0.661531	3.758396
890	0.686116	3.784589
900	0.619343	3.555765
910	0.592702	3.440224
920	0.559473	3.306068
930	0.526513	3.172719
940	0.558515	3.232955
950	0.542699	3.153306
960	0.520086	3.054757

Table 17 presents the range estimation for the "Short" transponder with its antenna matched to the measurement point and calculated relative to the datasheet point, using an Excel spreadsheet. The calculations for all other three prototypes are similar. All results are presented graphically in the Figure 45.

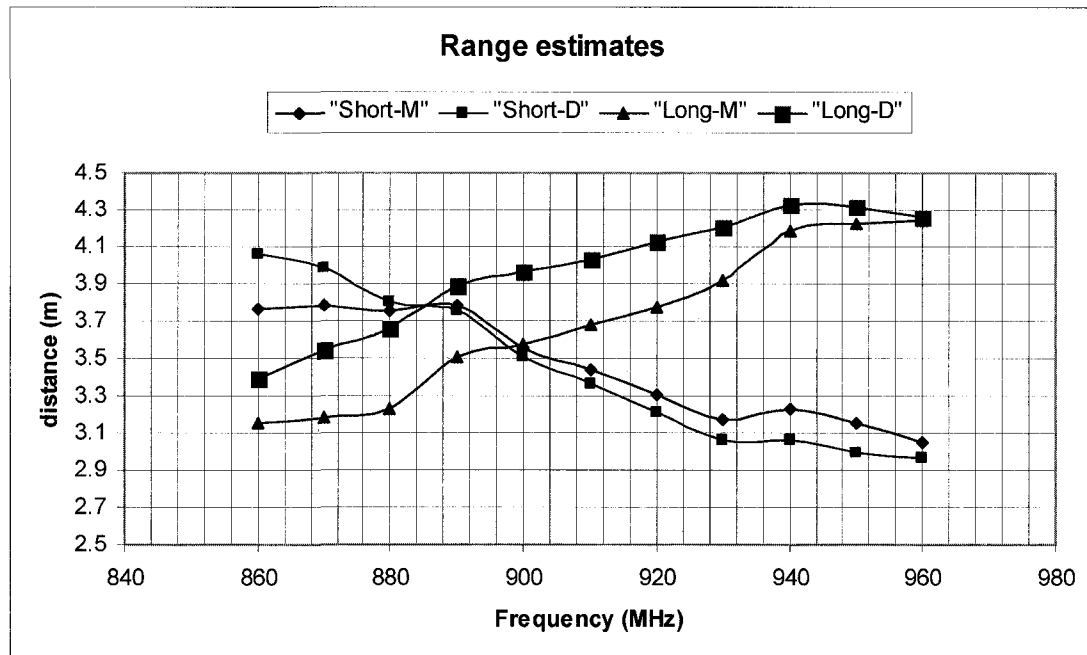


Figure 45 Range estimations for all four prototype transponders

Figure 45 presents the range estimations for transponders fabricated with all four antenna prototypes. These estimations are computed with measured values for antenna gain and mismatch power loss. The range estimation variation with frequency has the most influence due to impedance mismatch and wavelength variation in the 860 and 960 MHz interval.

3.6.2 Range Measurement

The prototype transponders were assembled. ASICs were attached with clear tape to antenna pads. The conductive epoxy, suitable for this process, was not available at the time of testing.

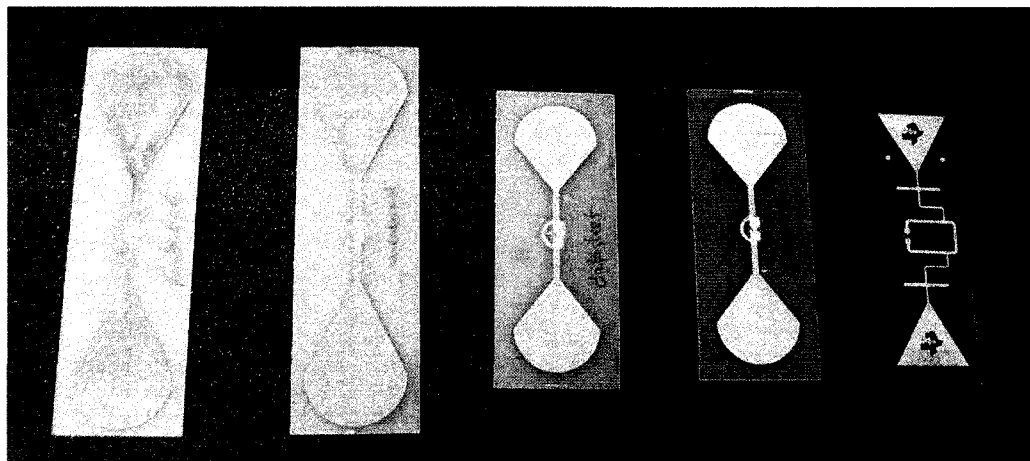


Figure 46 Prototype transponders

Figure 46 presents all four prototype transponders. The fifth transponder was fabricated by Texas Instruments and obtained as a sample.

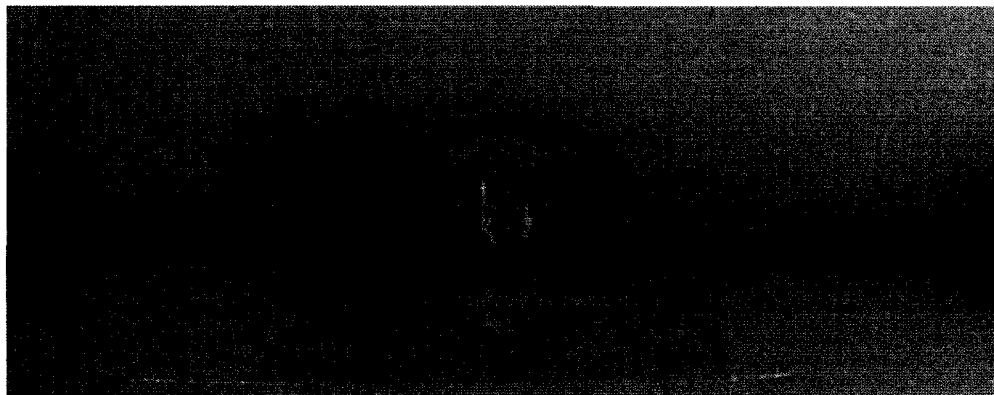


Figure 47 ASIC attachment to antenna

The RFID reader *INfinity* 9311-DK development kit manufactured by Sirit Inc. was used for the range measurement. Its main features are:

- Large variety of communications protocols
- Transmit power range: 2mW to 600 mW
- Transmit power increment step: 0.1 dB

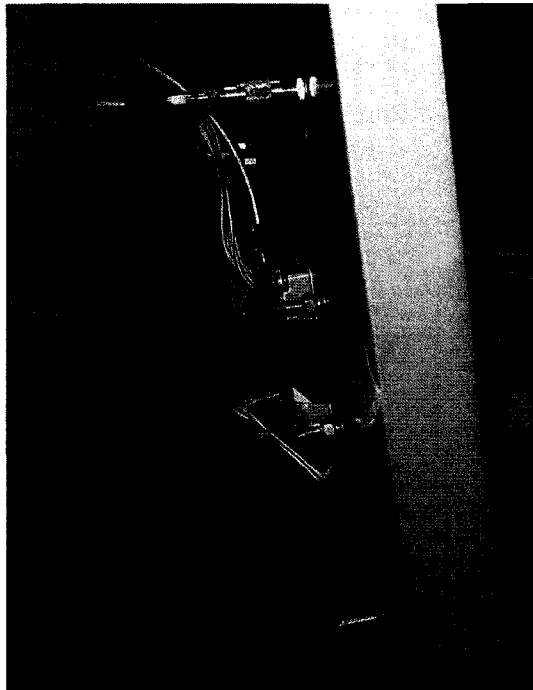


Figure 48 **Reader mounted to antenna**

As shown in Figure 48, in preparation for transponder range measurement, the reader was mounted to the back of the Symbol antenna in order to allow the use of a short coaxial cable for connection to the antenna port.

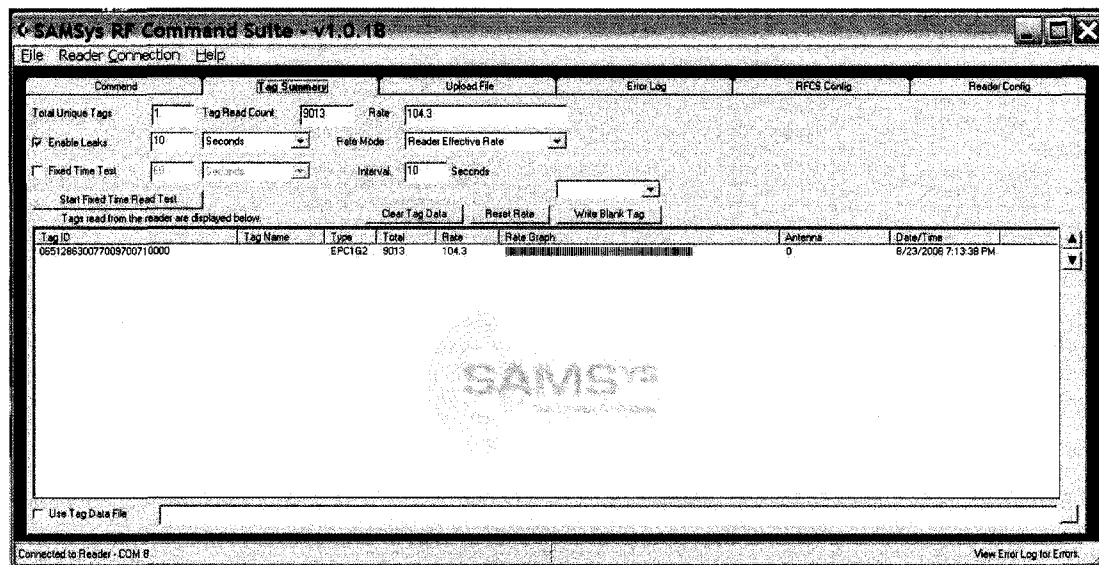


Figure 49 Reader's interface software control window

Figure 49 shows the window for communications software with the RFID reader. This interface software was installed on a computer, which was connected with the reader via a serial link. The Tag Summary Interface displays information about tags being read by the reader. This information includes the Tag ID, Tag Name, Type, Total Tags Read, and the Date/Time. Read rates, rate mode, and tag counts are also provided.

3.6.2.1 Setup and Calibration

The operations of transponders in close range from the reader's antenna are reliable. As the range increases, the degradation of the communications is gradual. The reader was set to interrogate the tag's population in continuous mode, via the interface software installed on the computer. In Figure 49 can be seen the "Rate" number displayed. This number is the average of all tags read count per second calculated by the software. This average can be calculated over any time interval and is always displayed "per second". This "Rate" indicator was considered a realistic performance parameter of transponders operating in the reader's field.

The observations made before testing showed this “Rate” indicator with values between 100 and 120 reads/second at short distance between reader and transponders. These values were approximate the same for all four transponder prototypes and were associated with 100% reliable operations.

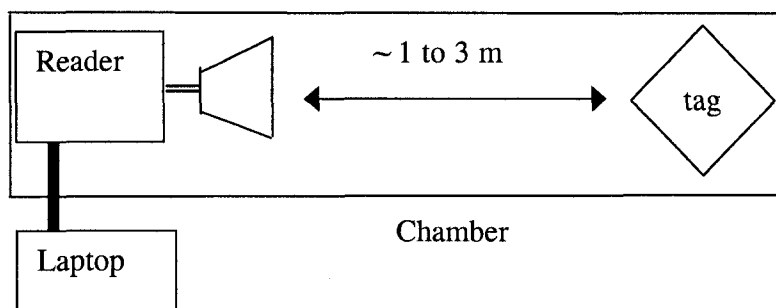


Figure 50 Setup for transponder range measurement

Figure 50 illustrates the setup used for transponder range measurement. Each test started with the transponder close to reader’s antenna and continued by gradually increasing the distance between them. The actual range measurement between reader’s antenna and transponder was taken while the “Rate” indicator displayed by the interface software was consistent between 50 and 80. The distance was then increased until the “Rate” dropped to zero in order to confirm the absence of field variations. The range determined by using this method represents a boundary where the communication between a reader and a transponder is approximate at half of maximum performance, which is expressed in reads/second.



Figure 51 Transponder during range measurement

Figure 51 shows the transponder held by a piece of tape from a wooden stool during range measurement. This support option was adopted as the least reflective hardware available in the laboratory at the time.

The reader's antenna facing the transponder inside the anechoic chamber was aligned for height and relative orientation in order to obtain the maximum directivity for both antennas.

The reader's transmit power was set to a value of +28 dBm using the interface software introduced in the section above. The actual direct and reflected power between reader and its antenna was verified using two calibrated RF power meters and a bi-directional coupler, described below.

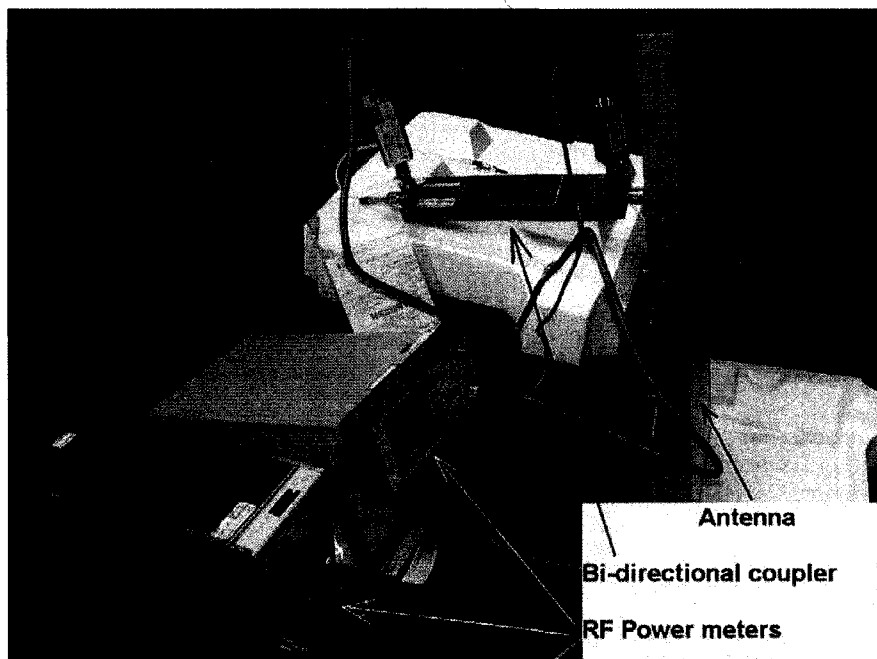


Figure 52 Direct and reflected power measurement of the reader assembly

Figure 52 shows the setup for power measurement between reader and antenna, using a bi-directional coupler of 20 dB nominal value attached to the antenna input port connector. Two power meters are attached to the coupler, one displaying average direct power into antenna port and second one displaying average reflected power from the same port. The time constant for these averages is approximate 100 ms.

First verification was the linearity of the reader's output power in 902 to 928 MHz frequency band. The method used two different known settings for reader's output power. These settings were downloaded into the reader the using the control features of the interface software.

Table 18 Reader's output power measurement for linearity verification

Reader setting (dBm)	22	28
Reader's output power (dBm)	19.7 to 21	25.7 to 27

Table 18 presents the results of the reader's output power measurement at 22 and 28 dBm settings. During the measurement, the average power was fluctuating between the minimum and the maximum levels presented in the table. The variations appear to be pseudo-random. The measurement results are lower than the settings with 1 to 2 dB for each power level. The relative difference between the two results is 6 dB, identical with the difference between 22 and 28 dBm settings. Therefore, the linearity was found adequate, even if an offset was identified in both settings.

There are two causes for power fluctuation. The first cause is associated with the frequency hopping during operations and variation of mismatch loss. The second is attributed to the sequence of "talk" and "listen" intervals. As explained in section 1.2.2, the reader's modulation is ASK with a 90% modulation level. Theoretically, the average power for a 50% duty cycle ASK modulated signal with 100% modulation level can be approximated to half of the maximum transmitted power (on the linear scale), which is equivalent to 3 dB lower than maximum transmitted power on a logarithmic scale.

Using the same setup as shown in Figure 52, the reflected power from antenna back to the reader was verified, while transmission power was set to +28 dBm.

Table 19 Direct and reflected power on antenna port at different frequencies

	866 – 868 MHz	902 – 928 MHz	952 – 954 MHz
Direct power in antenna port (dBm)	26 to 26.5	25.7 to 27	25 to 26.5
Reflected power from antenna port (dBm)	8.7 to 9.7	-0.3 to 1.2	0.7 to 1.7
Return loss Γ (dB) = Direct power - Reflected power	16.3 to 17.8	24.3 to 27.3	23.3 to 25.8

Table 19 presents the results of direct and reflected power measurement in reader's antenna port at different frequencies. The return loss is calculated in the last row. The average reflected power was fluctuating between the minimum and the maximum levels presented in this table. It was observed that the variation of the reflected power was not synchronized in time with the variation of the direct power. Also, the reflected power is noticeably higher for the 866 to 868 MHz frequency range compared with the other two frequency ranges. The highest reflected power is indicated by a return loss of 16.3 dB and is equivalent with a VSWR of 1.362:1. This result is within the antenna specifications, which has a VSWR of 2:1.

The measurement of the reader transmitted power concludes that a setting of 28 dBm is equivalent with an approximate effective power of 26 dBm. This power level was further used for the prototype transponders range measurement. The 26 dBm power level was used for range estimation in section 3.6.1.

3.6.2.2 Transponder's Range Measurement Results

The transponder's range measurement is described in section 3.6.2.1 and performed in accordance with the setup presented in Figure 50, using the anechoic chamber. Each one of the four prototype transponders was measured individually and the results are summarized in the following tables.

Table 20 Read range for "Short-D" tag

Reader's "Rate" (read count/sec)	866 – 868 MHz	902 – 928 MHz	952 – 954 MHz
50	2.55 m	2.8 m	2.65 m
80	2.45 m	2.7 m	2.55 m

Table 21 Read range for "Short-M" tag

Reader's "Rate" (read count/sec)	866 – 868 MHz	902 – 928 MHz	952 – 954 MHz
50	2.1 m	2.5 m	2.3 m
80	2.0 m	2.4 m	2.2 m

Table 22 Read range for "Long-D" tag

Reader's "Rate" (read count/sec)	866 – 868 MHz	902 – 928 MHz	952 – 954 MHz
50	2.45 m	2.8 m	2.6 m
80	2.35 m	2.7 m	2.5 m

Table 23 Read range for "Long-M" tag

Reader's "Rate" (read count/sec)	866 – 868 MHz	902 – 928 MHz	952 – 954 MHz
50	2.35 m	2.55 m	2.5 m
80	2.25 m	2.45 m	2.4 m

Tables 20 to 23 present the range measured between reader's antenna and each of all four prototype transponders while the "Rate" indicator (introduced in section 3.6.2.1) maintained values between 50 and 80 reads/second.

Table 24 Read range for Texas Instruments tag

Reader's "Rate" (read count/sec)	866 – 868 MHz	902 – 928 MHz	952 – 954 MHz
50	1.65 m	2.0 m	1.8 m
80	1.55 m	1.85 m	1.65 m

Tables 24 presents the range measurement for the Texas Instruments transponder (shown in the figure 46), done using the same setup.

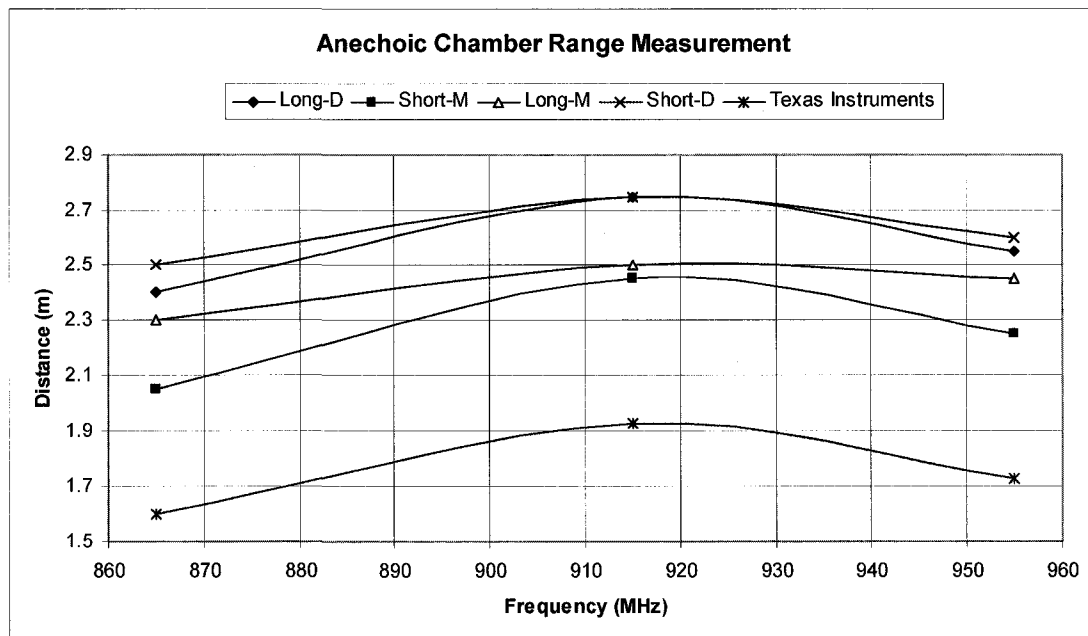
**Figure 53** Read range measurement for all four prototype transponders

Figure 53 illustrates the range measurement results for all four prototype transponders, including also the Texas Instruments tag. These results are based on the data presented on the Tables 20 to 24.

3.6.2.3 Range of Prototype Transponders in Real Environment

The setup for this test is similar with the setup presented in section 3.6.2.1, with the difference that all transponders were operated simultaneously. In this particular test the power of the transmitter was set to +28 dBm (equivalent with +26 dBm effective, as measured in section 3.6.2.1).

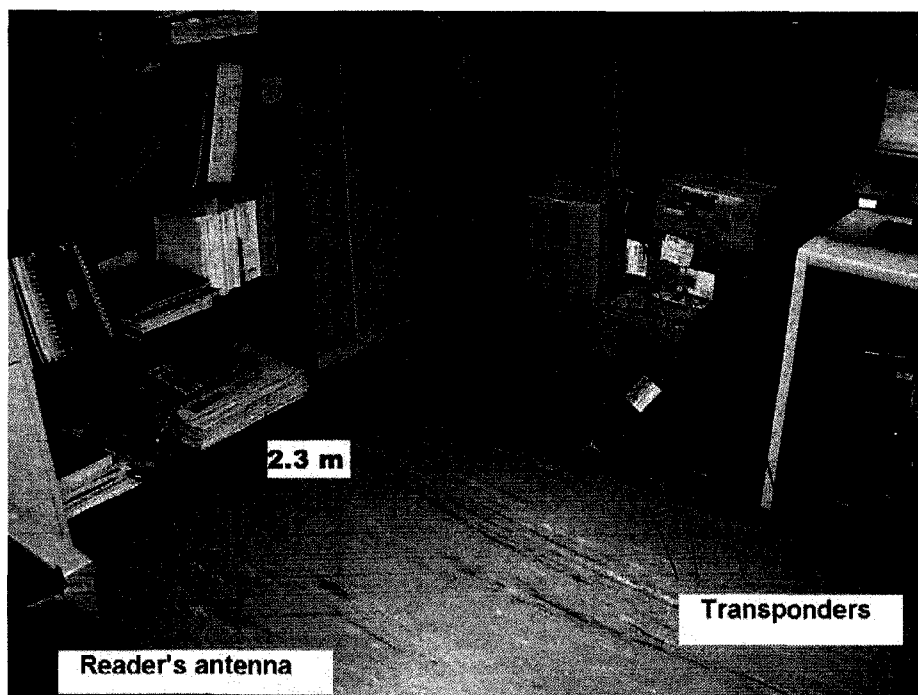


Figure 54 RFID system operations in real environment

As seen in Figure 54, all four prototypes and the Texas Instruments tag were attached to cardboard boxes and placed in front of the reader. The office environment was located in a concrete building. There were multiple metallic surfaces around testing area and multipath interference was detected during testing. When all transponders were moved towards the reader with an approximate distance of $\lambda/4$ (80 to 90 mm), three tags showed intermittent operations.

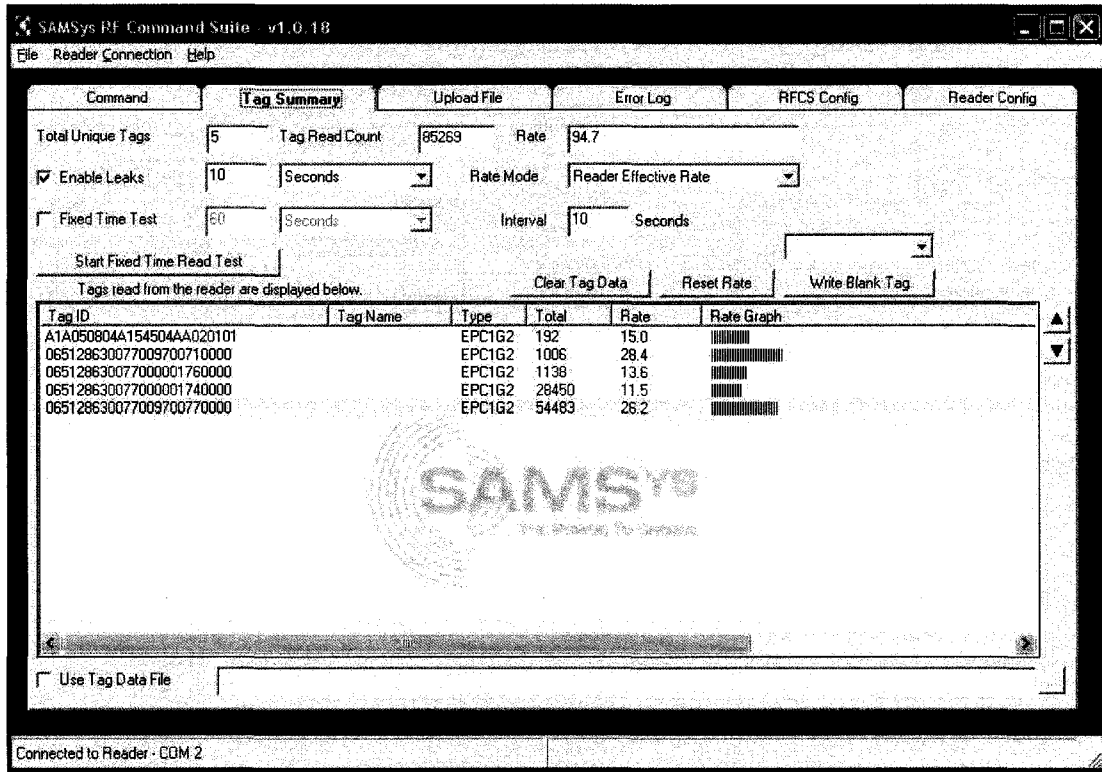


Figure 55 Reader operating with all tags in real environment

Figure 55 presents simultaneous operations of all five transponders. As seen in the figure, the total read "Rate" is the sum of the individual rates of respective tags. In time, these individual rates were not constant, showing variations of ± 10 reads/sec.

Table 25 Range of prototype transponders in real environment

Prototype	866 – 868 MHz	902 – 928 MHz	952 – 954 MHz
"Long-D"	2.0 to 2.1 m	2.2 to 2.3 m	2.0 to 2.1 m
"Short-D"	2.1 to 2.2 m	2.2 to 2.3 m	2.1 to 2.2 m

Table 25 presents the range measurement in real environment setup shown in Figure 54. It is pointed out that each particular environment may render different results.

3.6.2.4 Analysis of Range Measurement Results

The operation of the transponders in a real environment shows a relative degradation of performance in comparison with anechoic chamber function, which was expected. The results obtained in a real environment show that both "Short-D" and "Long-D" prototype transponders satisfy the range requirement. However, these results are subject to multipath interference specific to each particular environment.

The focus of the analysis is on the range measurement results obtained in the anechoic chamber. These results are referenced to the range estimation results presented in section 3.6.1. The reference Figures 45 and 53 contain the presentation of estimated and measured performance for all four prototype transponders in graphical format.

All four prototype transponders recorded a better range than the sample tag from Texas Instruments. As seen in Figure 46, the size and shape for this sample tag are closer to the "Short" prototype transponder. The matching impedance for the design of this sample transponder is unknown. The range difference may be explained if the design included a specific object in close proximity, which was not present during testing.

The prototypes "-D" have better ranges than the prototypes "-M". This result was expected, as the ASIC's datasheet impedance is more accurate than the measured impedance. This result is in agreement with the prototype antenna impedance measurement results presented in section 3.5.1.1.

The overall performance of the "Short-D" prototype transponder is slightly better than the "Long-D" prototype at both ends of the frequency band. This fact can be explained by a better reactance match at low and high frequencies, at the expense of resistance.

The measured range of both "Long" prototype transponders have similar frequency variation (approximately the same trend) compared with the estimated range. However,

the estimated range variation with frequency (trend) of both "Short" prototypes is completely different than the measured range. This result may indicate errors in range estimation.

The overall measured range performance for all four prototype transponders is lower than the estimated performance. The difference between the estimated and measured range suggests that there is room for improvement in prototype assembly and accuracy of measurement. This improvement could increase the present average measured range for "-D" prototypes from an average of 2.6 m to approximately 3 m. At the same time, the difference also suggests that there are multiple unaccounted losses in the range estimation. These losses could lower the average estimated range from 3.7 m to approximate 3 m. Subsequently, both estimation and prototype measurement stages can have closer results. Potential sources of error and/or improvement are presented, as follows:

1. The proximity of transponder to the wooden stool during range measurement suggests that a different setup could be used inside the anechoic chamber.

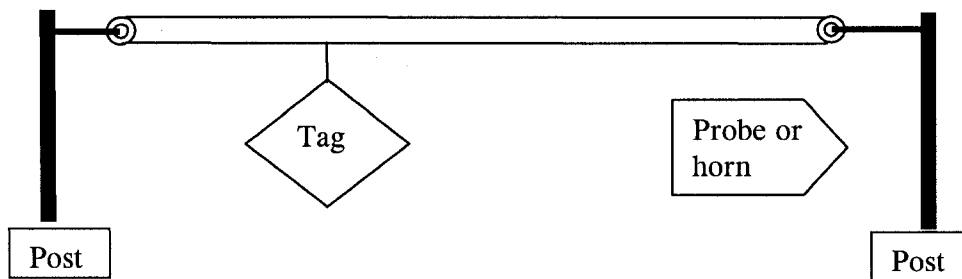


Figure 56 Recommended range measurement setup

Figure 56 presents a recommended range measurement setup for transponders. The probe is connected to the reader and the transponder can be moved along a string, providing a convenient range adjustment.

2. Another source of error for range estimation is the constant gain of the reader

antenna. Transponder range measurement inside the anechoic chamber could be repeated using either a pyramidal horn or the chamber's probe attached to the reader, replacing the present Symbol antenna. These antennas could also have the impedance measured and the gain adjusted with the power transmission coefficient.

By using these linearly polarized antennas, the gain uncertainty considered for the circular polarized antenna can be also avoided.

3. The prototype antennas impedance measurements could be more accurate. It was shown in section 3.5.1.2 that objects in vicinity of antenna and VNA's calibration using the SMA connector as a probe can offset impedance measurement results.

4 CONCLUSIONS

This project presents the antenna design for UHF RFID transponder, operating in 860 to 960 MHz frequency band. Measurement results show good performance of the prototype transponders. The range requirement was satisfied by two different prototypes.

The concept and physics of the backscattering RFID system was presented. A summary description of the modulation type, data encoding, data rate and integrity implemented in EPC™ Radio-Frequency Identity Protocol, Class-1 Generation-2 UHF RFID (Protocol for Communications) was also presented. Various factors affecting the performance of the transponder were further analyzed for real operational conditions, highlighting issues that must be addressed during the design process, including but not limited to orientation, cost, antenna modeling for a specific object and transponder density in the reader's field.

The fundamental parameters of the antenna, and the relationship between them, were studied. The results determined for classic antenna geometries were used as references and software simulation tools were further employed to finalize the design. As well, special attention was given to techniques that improve broadband antenna performance. As a result, the shape of antennas considered for this design is a variation of the bow-tie geometry.

The design procedure required a thorough verification of the results at each stage. This verification was comprised of either an actual measurement or a comparison with other published results. The design process was not linear and required several iterations until target performance was achieved. This approach ensured reliable incremental progress and provided data for estimation of the prototype's performance.

Two different impedance matching points were considered with the purpose to build prototypes that have small differences between parameters. This way, the relative

performance of the prototypes and their sensitivity could be compared.

The parametric study of the bow-tie antenna using the Ansoft HFSS software package searched for two main parameters that could be used to control the antenna impedance, targeting the desired matching point in nearly orthogonal directions. Even if the parameters exhibited a small interference between the impedance variations produced by one and other, the target matching point was achieved after multiple iterations.

Furthermore, the bandwidth for the operation of transponders required the reactance variation to be small between 860 to 960 MHz. Equally, the length of the trace of antenna impedance on the Smith Chart must be as short as possible. The interpretation of results for impedance on the Smith Chart provided a means of controlling the parameters for adjustments in the desired direction. The final results of the parametric study revealed two suitable antenna models:

- “Short” model, of approximate $\lambda/4$ length
- “Long” model, of approximate $\lambda/3$ length

These two antenna models were matched at two different impedance points respectively, producing four options for prototyping. The design did not take into consideration the transponder’s proximity to other objects.

The results of the impedance measurements for all four antenna prototypes indicated a close match to the expected impedance, which was previously obtained in simulations. The gain measurements of the two antenna prototypes (“Long” and “Short”) were found within the expected interval of 1.5 to 1.9 dBi, which is appropriate for their respective physical size. All measurements included the study of encountered errors by type and magnitude. In this way, the measurement accuracy was clearly defined. In order to lower the uncertainty interval and increase the accuracy, a need for a calibrated antenna standard with impedance and gain variations known in the 860 to 960 MHz frequency band was identified.

The intermediate results obtained from impedance and gain measurements were used to estimate the operation range of the prototype transponders. In the end, this estimation proved to be too optimistic, due to various errors contained in the prototype antennas measured data. Also, the assumption of constant gain for the reader's antenna introduced an error. The input impedance variation with frequency for the reader's antenna was found to be adequate. The verification of this input impedance was performed by measurement of direct and reflected power into the antenna port.

The range measurement of "Long-D" and "Short-D" prototype transponders in a real environment was found to satisfy the 2 m requirement. Inside the anechoic chamber the respective ranges were above 2.4 m and peaked at 2.8 m; however, these results were below the estimated ranges. The analysis concluded that the measured range can be improved by using a different setup inside the anechoic chamber, with a linearly polarized antenna connected to the reader. The estimated range can be corrected by knowing the reader's antenna gain and impedance variation with frequency.

The range of transponders with antennas properly matched (ASIC's datasheet conjugate impedance) is superior to the other variants. The analysis of these results concludes high sensitivity of the design to the impedance matching point, resulting in a significant impact on range performance.

Future research would include the correction of the range estimation and improvement of the measurement accuracy. Fine tuning of the design procedure and elimination of various identified sources of error are considered essential for further developments. Additionally, the prototype antennas can be trimmed for best performance. The next stage of development would include parametric analysis of an antenna model in proximity of objects made from different materials, such as plastic, water or metal.

BIBLIOGRAPHY

- [1] K. Finkenzeller; *RFID Handbook: Radio-Frequency Identification Fundamentals and Applications*, 2nd ed: Wiley, 2004.
- [2] *EPC™ Radio-Frequency Identity Protocols; Class-1 Generation-2 UHF RFID Protocol for Communications at 860 MHz – 960 MHz*, Version 1.0.9
- [3] Motorola; *Understanding Gen 2: What It Is, How You Will Benefit And Criteria For Vendor Assessment*, White Paper
- [4] C. A. Balanis; *Antenna Theory - Analysis and Design* , Third Edition, Wiley, 2005
- [5] R. Ludwig, P. Bretchko; *RF Circuit Design – Theory and Applications*, Prentice-Hall, 2000
- [6] K. V. Seshagiri Rao, Pavel V. Nikitin, Sander F. Lam; *Antenna Design for UHF RFID Tags: A Review and a Practical Application*, IEEE Transactions on Antennas and Propagation, VOL. 53, NO. 12, Dec 2005
- [7] K. V. Seshagiri Rao, Pavel V. Nikitin, Sander F. Lam, Vijay Pillai, Rene Martinez and Harley Heinrich; *Power Reflection Coefficient Analysis for Complex Impedances in RFID Tag Design*, IEEE Transactions on Microwave Theories and Techniques, VOL. 53, NO. 9, Sept 2005
- [8] K. Kurokawa; *Power Waves and the Scattering Matrix*, IEEE Transactions on Antennas and Propagation, March 1965
- [9] Texas Instruments; *RI-UHF-STRAP-08, Datasheet*
- [10] Texas Instruments; *UHF Gen2 IC Antenna Design – Reference Guide*, October 2006
- [11] Texas Instruments; *UHF Gen 2 System Overview*, September 2005
- [12] M. Laudien; *Radio Frequency Identification (RFID) Antenna and System Design*, Ansoft Corporation
- [13] *IEEE Standard Test Procedures for Antennas*, ANSI/IEEE Std 149-1979
- [14] Matrics Inc.; *Passive RFID – A Primer for New RF Regulations*; White Paper

- [15] Sirit; *INfinity 9311-DK UHF Reader Module Evaluation Kit*, Datasheet
- [16] www.epcglobalinc.org/home
- [17] www.matrics.com
- [18] www.aimglobal.org
- [19] www.ieee.org
- [20] www.rfcafe.com
- [21] <http://www.ti.com/rfid/shtml/doc-center-brochures.shtml>
- [22] <http://www.alientechnology.com>
- [23] <http://www.intermec.com>
- [24] <http://www.impinj.com/>

APPENDIX 1 Conversion of impedance from Parallel to Series configuration

The die Parallel impedance available on the datasheet at -13 dBm power level is converted to Series impedance.

The formula used for reactance calculation: $X_c = \frac{1}{2\pi fC}$

The formula used for series impedance $\frac{1}{Z} = \frac{1}{R} + \frac{1}{j} \cdot X_c$

Xc	Cap (pF)	Res (ohm)	Freq (MHz)	Series Impedance
66.09424547	2.800	440.000	860.000	9.70921221044044-64.6357839810613j
65.3345415	2.800	440.000	870.000	9.49208209752718-63.9250850634223j
64.59210353	2.800	440.000	880.000	9.28210379011404-63.229488507181j
63.86634956	2.800	380	890.000	10.4390988846705-62.1118570858324j
63.15672345	2.800	380	900.000	10.2146087932411-61.459036021017j
62.46269352	2.800	380	910.000	9.9972191148058-60.8193955379102j
61.7837512	2.800	380	920.000	9.78663619599064-60.1925535796894j
61.11940979	2.800	380	930.000	9.58258127154416-59.5781421274702j
58.38405836	2.9	340	940.000	9.73842608881686-56.7117970753033j
57.76948933	2.9	340	950.000	9.54020809601582-56.1485100615332j
57.16772381	2.9	340	960.000	9.34792500965314-55.5959602965537j

APPENDIX 2 Calculation of ASIC impedance using Parallel configuration

The chip and tabs impedances correspond to -13 dBm power level.

The formula used for tabs impedance: $Z_p = R_p + \frac{j}{2\pi f C_p}$

where $R_p = 3.5$ ohm and $C_p = 0.095$ pF

The formula used for total impedance: $\frac{1}{Z_T} = \frac{1}{Z_{Die}} + \frac{1}{Z_p}$

Frequency	Die impedance	Package	TOTAL
860.000	9.70921221044044-64.6357839810613j	3.5-1948.04091911745j	9.09894428497392-62.6028807724472j
870.000	9.49208209752718-63.9250850634223j	3.5-1925.64964418506j	8.895262389794-61.9125590951358j
880.000	9.28210379011404-63.229488507181j	3.5-1903.76726186478j	8.69830170699617-61.2369722591559j
890.000	10.4390988846705-62.1118570858324j	3.5-1882.37661847304j	9.7860509049122-60.1792095269866j
900.000	10.2146087932411-61.459036021017j	3.5-1861.46132271223j	9.57531976219701-59.5444260591019j
910.000	9.9972191148058-60.8193955379102j	3.5-1841.00570378132j	9.37126919850187-58.9225318000018j
920.000	9.78663619599064-60.1925535796894j	3.5-1820.99477221848j	9.17362212767893-58.3131500217157j
930.000	9.58258127154416-59.5781421274702j	3.5-1801.4141832699j	8.98211556073407-57.7159180066598j
940.000	9.73842608881686-56.7117970753033j	3.5-1782.25020259681j	9.15002852363656-55.0101956049859j
950.000	9.54020809601582-56.1485100615332j	3.5-1763.48967414842j	8.96353180750619-54.4618233250964j
960.000	9.34792500965314-55.5959602965537j	3.5-1745.11999004271j	8.78263204635502-53.9239642550107j

APPENDIX 3 Calculation of datasheet reflection coefficient

The ASIC impedance corresponds to -13 dBm power level.

The formula used: $\Gamma = \frac{Z_A - Z_0}{Z_A + Z_0}$

	Zref			
	Re	Im	Complex	
	50	0	50	
F (MHz)	R _L (Ω)	X _L (Ω)	Cplx	Reflection Coefficient
860.000	9.099	-62.603	9.09894428497392-62.6028807724472j	0.202637722717173-0.84463734811377j
870.000	8.895	-61.913	8.895262389794-61.9125590951358j	0.193416335267874-0.847906211494401j
880.000	8.698	-61.237	8.69830170699617-61.2369722591559j	0.184231126852479-0.851050446130088j
890.000	9.786	-60.179	9.7860509049122-60.1792095269866j	0.169166123080263-0.836297517639912j
900.000	9.575	-59.544	9.57531976219701-59.5444260591019j	0.160290952773126-0.839273603118561j
910.000	9.371	-58.923	9.37126919850187-58.9225318000018j	0.151452602355994-0.84213394283896j
920.000	9.174	-58.313	9.17362212767893-58.3131500217157j	0.142652451734577-0.844880445122631j
930.000	8.982	-57.716	8.98211556073407-57.7159180066598j	0.133891820176962-0.847515017329122j
940.000	9.150	-55.010	9.15002852363656-55.0101956049859j	9.34649649610826E-002-0.843087836894886j
950.000	8.964	-54.462	8.96353180750619-54.4618233250964j	8.48134500695591E-002-0.84531449633197j
960.000	8.783	-53.924	8.78263204635502-53.9239642550107j	7.62083818298157E-002-0.847435789503346j

APPENDIX 4 Measurement of ASIC impedance at five power levels

Below is presented the measurement only for one ASIC.

IC1	-10 dBm		-11 dBm		-12 dBm	
F (MHz)	R (ohm)	X (ohm)	R (ohm)	X (ohm)	R (ohm)	X (ohm)
860	3.61E+00	-5.50E+01	3.52E+00	-5.49E+01	3.53E+00	-5.43E+01
870	3.52E+00	-5.42E+01	3.41E+00	-5.42E+01	3.53E+00	-5.35E+01
880	3.48E+00	-5.33E+01	3.38E+00	-5.33E+01	3.47E+00	-5.27E+01
890	3.35E+00	-5.25E+01	3.31E+00	-5.25E+01	3.40E+00	-5.19E+01
900	3.28E+00	-5.17E+01	3.19E+00	-5.17E+01	3.28E+00	-5.11E+01
910	3.23E+00	-5.08E+01	3.13E+00	-5.08E+01	3.20E+00	-5.02E+01
920	3.15E+00	-5.00E+01	3.08E+00	-5.00E+01	3.18E+00	-4.94E+01
930	3.09E+00	-4.92E+01	3.00E+00	-4.92E+01	3.08E+00	-4.86E+01
940	2.99E+00	-4.84E+01	2.90E+00	-4.84E+01	3.00E+00	-4.79E+01
950	2.94E+00	-4.76E+01	2.85E+00	-4.76E+01	2.90E+00	-4.71E+01
960	2.86E+00	-4.69E+01	2.75E+00	-4.69E+01	2.80E+00	-4.63E+01

-13 dBm		-14 dBm	
R (ohm)	X (ohm)	R (ohm)	X (ohm)
3.46E+00	-5.42E+01	3.41E+00	-5.46E+01
3.38E+00	-5.35E+01	3.32E+00	-5.38E+01
3.30E+00	-5.27E+01	3.28E+00	-5.29E+01
3.21E+00	-5.19E+01	3.17E+00	-5.20E+01
3.14E+00	-5.10E+01	3.11E+00	-5.13E+01
3.10E+00	-5.01E+01	3.06E+00	-5.04E+01
3.05E+00	-4.94E+01	3.00E+00	-4.96E+01
2.98E+00	-4.86E+01	2.94E+00	-4.88E+01
2.88E+00	-4.78E+01	2.84E+00	-4.80E+01
2.82E+00	-4.71E+01	2.78E+00	-4.72E+01
2.71E+00	-4.63E+01	2.72E+00	-4.65E+01

APPENDIX 5 Measured ASIC impedance

Four ASICs impedance were measured at -13 dBm and the average was calculated.

F (MHz)	IC1		IC2		IC3	
	R (ohm)	X (ohm)	R (ohm)	X (ohm)	R (ohm)	X (ohm)
860	3.46E+00	-5.42E+01	3.32E+00	-5.41E+01	3.13E+00	-5.26E+01
870	3.38E+00	-5.35E+01	3.22E+00	-5.33E+01	3.07E+00	-5.19E+01
880	3.30E+00	-5.27E+01	3.12E+00	-5.25E+01	3.05E+00	-5.11E+01
890	3.21E+00	-5.19E+01	3.06E+00	-5.17E+01	2.97E+00	-5.03E+01
900	3.14E+00	-5.10E+01	3.03E+00	-5.09E+01	2.93E+00	-4.95E+01
910	3.10E+00	-5.01E+01	2.97E+00	-5.01E+01	2.88E+00	-4.87E+01
920	3.05E+00	-4.94E+01	2.90E+00	-4.93E+01	2.78E+00	-4.79E+01
930	2.98E+00	-4.86E+01	2.83E+00	-4.85E+01	2.72E+00	-4.71E+01
940	2.88E+00	-4.78E+01	2.75E+00	-4.77E+01	2.61E+00	-4.64E+01
950	2.82E+00	-4.71E+01	2.69E+00	-4.69E+01	2.57E+00	-4.56E+01
960	2.71E+00	-4.63E+01	2.60E+00	-4.62E+01	2.50E+00	-4.49E+01

IC4	
R (ohm)	X (ohm)
3.73E+00	-5.34E+01
3.61E+00	-5.27E+01
3.56E+00	-5.18E+01
3.48E+00	-5.10E+01
3.41E+00	-5.02E+01
3.40E+00	-4.94E+01
3.28E+00	-4.86E+01
3.22E+00	-4.78E+01
3.15E+00	-4.70E+01
3.08E+00	-4.63E+01
3.04E+00	-4.56E+01

Average 1-4	
R (ohm)	X (ohm)
3.41E+00	-5.36E+01
3.32E+00	-5.28E+01
3.26E+00	-5.20E+01
3.18E+00	-5.12E+01
3.13E+00	-5.04E+01
3.09E+00	-4.96E+01
3.00E+00	-4.88E+01
2.94E+00	-4.80E+01
2.85E+00	-4.72E+01
2.79E+00	-4.65E+01
2.71E+00	-4.57E+01

APPENDIX 6 Measurement of the prototype antennas impedance

The measurement of impedance is relative to 50 ohm.

FREQUENCY MHz	"Short-M"			"Short-D"	
	Resistance	Reactance		Resistance	Reactance
860	1.97E+01	4.53E+01		2.44E+01	5.36E+01
870	2.09E+01	4.62E+01		2.66E+01	5.56E+01
880	2.35E+01	4.71E+01		3.04E+01	5.57E+01
890	2.77E+01	4.70E+01		3.50E+01	5.53E+01
900	3.08E+01	4.30E+01		4.05E+01	5.18E+01
910	3.02E+01	4.04E+01		4.18E+01	4.70E+01
920	3.17E+01	3.81E+01		4.39E+01	4.32E+01
930	3.03E+01	3.48E+01		4.33E+01	3.66E+01
940	2.92E+01	3.40E+01		4.07E+01	3.30E+01
950	2.92E+01	3.27E+01		3.72E+01	3.03E+01
960	2.88E+01	3.08E+01		3.42E+01	2.94E+01

FREQUENCY MHz	"Long-M"			"Long-D"	
	Resistance	Reactance		Resistance	Reactance
860	1.00E+01	4.08E+01		1.17E+01	4.22E+01
870	9.64E+00	4.14E+01		1.17E+01	4.40E+01
880	9.00E+00	4.26E+01		1.17E+01	4.53E+01
890	9.05E+00	4.39E+01		1.19E+01	4.63E+01
900	8.79E+00	4.48E+01		1.18E+01	4.73E+01
910	8.76E+00	4.58E+01		1.14E+01	4.84E+01
920	8.39E+00	4.70E+01		1.13E+01	4.98E+01
930	8.50E+00	4.84E+01		1.15E+01	5.12E+01
940	8.87E+00	4.93E+01		1.14E+01	5.23E+01
950	8.95E+00	5.00E+01		1.11E+01	5.37E+01
960	8.66E+00	5.09E+01		1.11E+01	5.52E+01

APPENDIX 7 Measurement of transmission level from horn to probe

This measurement was done in the anechoic chamber. This data was used for maximum gain calibration.

FREQUENCY MHz	Probe Transmitting dB	Horn Transmitting dB	Average dB
860	-32.031	-32.161	-32.096
870	-32.192	-32.285	-32.2385
880	-32.268	-32.353	-32.3105
890	-32.358	-32.414	-32.386
900	-32.485	-32.455	-32.47
910	-32.597	-32.481	-32.539
920	-32.781	-32.601	-32.691
930	-33.005	-32.867	-32.936
940	-33.157	-33.092	-33.1245
950	-33.354	-33.293	-33.3235
960	-33.476	-33.367	-33.4215

APPENDIX 8 Transmission coefficient for antennas relative to 50 ohm

Calculation of reflection and transmission coefficients for "Short-M" and "Long-M" antennas. This data was used for maximum gain calculation.

FREQUENCY	"Short-M"	
MHz	Gamma	Transmission coefficient (dB)
860	-8.76985994939533E-003+0.655916137515967j	-2.44E+00
870	1.0023886301967E-002+0.64486642025533j	-2.34E+00
880	3.58127085836409E-002+0.618135036643082j	-2.10E+00
890	5.74689233383582E-002+0.569486534116122j	-1.72E+00
900	3.58676951308729E-002+0.512809437141082j	-1.33E+00
910	4.99924517524303E-003+0.500900519674008j	-1.25E+00
920	-5.45872364942239E-003+0.468924413979798j	-1.08E+00
930	-4.83974666602535E-002+0.454543650121559j	-1.02E+00
940	-6.66721279762327E-002+0.457520465288283j	-1.04E+00
950	-7.79651212578111E-002+0.445234634930985j	-9.93E-01
960	-0.100991853024736+0.431019221306787j	-9.47E-01

FREQUENCY	"Long-M"	
MHz	Gamma	Transmission coefficient (dB)
860	-0.140287686857847+0.774454729168625j	-4.20E+00
870	-0.131590798968887+0.785478282904923j	-4.37E+00
880	-0.113261731268938+0.804771608888684j	-4.69E+00
890	-9.08337201770698E-002+0.810817202251219j	-4.76E+00
900	-7.5406170579739E-002+0.820295120009722j	-4.93E+00
910	-5.84321288848146E-002+0.825196533126169j	-5.01E+00
920	-3.91858760675584E-002+0.836508271915954j	-5.25E+00
930	-1.48243419722544E-002+0.839636633942659j	-5.30E+00
940	1.26816008452198E-003+0.836100794246124j	-5.22E+00
950	1.3855047922299E-002+0.836859529875408j	-5.24E+00
960	2.76812961807313E-002+0.843917642355998j	-5.42E+00

APPENDIX 9 Transmission level from prototype antennas to probe

This measurement was done in the anechoic chamber. This data was used for maximum gain calculation.

"Short-M"

FREQUENCY	Probe Transmitting	Prototype Transmitting	Average
Hz	dB	dB	dB
860	-40.318	-40.08	-40.199
870	-40.1	-39.849	-39.9745
880	-39.803	-39.599	-39.701
890	-39.422	-39.366	-39.394
900	-39.225	-39.2	-39.2125
910	-39.185	-39.155	-39.17
920	-39.193	-38.961	-39.077
930	-39.127	-38.881	-39.004
940	-39.194	-39.044	-39.119
950	-38.957	-39.035	-38.996
960	-39.08	-39.102	-39.091

"Long-M"

FREQUENCY	Probe Transmitting	Prototype Transmitting	Average
Hz	dB		
860	-41.055	-41.517	-41.286
870	-41.459	-41.874	-41.6665
880	-41.621	-42.056	-41.8385
890	-41.523	-42.041	-41.782
900	-41.842	-42.307	-42.0745
910	-42.046	-42.405	-42.2255
920	-42.211	-42.269	-42.24
930	-42.468	-42.271	-42.3695
940	-42.819	-42.561	-42.69
950	-42.793	-42.693	-42.743
960	-43.081	-42.951	-43.016